The effect of white matter hyperintensities on regional brain volumes and white matter microstructure, a population-based study in HUNT

Torgil Riise Vangberg [a,b], Live Eikenes [d], Asta K. Håberg [c,e,*]

[a] Medical Imaging Research Group, Department of Clinical Medicine, UiT the Arctic University of Norway, Tromsø, Norway
[b] PET Center, University Hospital North Norway, Tromsø, Norway
[c] Department of Radiology and Nuclear Medicine, St. Olav University Hospital, Trondheim, Norway
[d] Department of Circulation and Medical Imaging, Norwegian University of Science and Technology (NTNU), Trondheim, Norway
[e] Department of Neuromedicine and Movement Science, Norwegian University of Science and Technology (NTNU), Trondheim, Norway

ARTICLE INFO

ABSTRACT

Even though age-related white matter hyperintensities (WMH) begin to emerge in middle age, their effect on brain micro- and macrostructure in this age group is not fully elucidated. We have examined how presence of WMH and load of WMH affect regional brain volumes and microstructure in a validated, representative general population sample of 873 individuals between 50 and 66 years. Presence of WMH was determined as Fazakas grade ≥ 1. WMH load was WMH volume from manual tracing of WMHs divided on intracranial volume. The impact of age appropriate WMH (Fazakas grade 1) on the brain was also investigated. Major novel findings were that even the age appropriate WMH group had widespread macro- and microstructural changes in gray and white matter, showing that the mere presence of WMH, not just WMH load is an important clinical indicator of brain health. With increasing WMH load, structural changes spread centrifugally. Further, we found three major patterns of FA and MD changes related to increasing WMH load, demonstrating a heterogeneous effect on white matter microstructure, where distinct patterns were found in the proximity of the lesions, in deep white matter and in white matter near the cortex. This study also raises several questions about the onset of WMH related pathology, in particular, whether some of the aberrant brain structural and microstructural findings are present before the emergence of WMH. We also found, similar to other studies, that WMH risk factors had low explanatory power for WMH, making it unclear which factors lead to WMH.

1. Introduction

White matter hyperintensities (WMH) are common on brain MRI in middle-aged and older adults in both hospital (Gouw et al., 2006; Tuladhar et al., 2014; van der Veen et al., 2014) and general populations (Håberg et al., 2016; Vernooij et al., 2007). WMH constitute focal hyperintense lesions in cerebral white matter on T2-weighted or fluid-attenuated inversion recovery (FLAIR) images. Histological studies of WMH report evidence of small vessel disease, amyloid angiopathy, ischemic hypoxic injury, changes in the blood brain barrier properties, axonal pathology such as demyelination and axonal loss, as well as neuroinflammation with activated microglia and astrocytes (Fazekas et al., 1993; Fernando et al., 2006; Gouw et al., 2011; Murray et al., 2012; Scott et al., 2015; Simpson et al., 2007). Likewise, MRI studies are consistent with the histological findings demonstrating reduced myelin density (Bastin et al., 2009; Fazekas et al., 2005), lower fractional anisotropy (FA) and/or higher mean diffusivity (MD) (Bastin et al., 2009; van Leijsen et al., 2018; Leritz et al., 2014; Maniega et al., 2015; Vernooij et al., 2008) in WMH compared to normal appearing white matter. Clinical data support an association between WMH and cerebrovascular disease (Jeerakathil et al., 2004), cardiovascular risk factors (Dickie et al., 2016b; van Dijk et al., 2004; van Dijk et al., 2008), and neurodegeneration with a higher risk of Alzheimer's disease (Brickman et al., 2012; Lee et al., 2016; Lindemer et al., 2015) and other dementias (O'Brien and Thomas, 2015) in people with extensive WMH. Clinically, WMH is also associated with impaired motor (de Laat et al., 2011; Sachdev, 2005; Willey et al., 2013) and cognitive functioning (Brickman et al., 2011; Maillard et al., 2012; Murray et al., 2010), depression (van Agtmaal et al., 2017; Wang et al., 2014a) and higher mortality (Debette and Markus, 2010).

Both histological and MRI studies have revealed that normal-appearing white matter surrounding WMH is also altered. Histological studies show microglia activation in normal-appearing white matter (Al-Mashhadi et al., 2015; Simpson et al., 2007). MRI studies have demonstrated decreased FA and increased MD (Leritz et al., 2014; Maniega et al., 2015; Taylor et al., 2007), and changes in perfusion (Promjunyakul et al., 2015). This affection of apparently normal white matter has been referred to as the penumbra of WMH (Maillard et al., 2011). The extent and structural aberrance of such a penumbral zone remain largely unknown due to extensive use of region of interest approaches and predefined histological sections, but the largest changes are reported immediately surrounding the WMH (Maillard et al., 2011; Promjunyakul et al., 2015). Thus, WMH is considered a localized manifestation of more widespread white matter pathology (Al-Mashhadi et al., 2015; Simpson et al., 2007) where the surrounding white matter is at risk of evolving into WMH (Maillard et al., 2014). In addition, pathological changes may spread along the axons crossing the WMH possibly by anterograde or Wallerian degeneration (McAleese et al., 2017; Wardlaw et al., 2015). Cortical thinning in the temporal and frontal lobes (Dickie et al., 2016a; Tuladhar et al., 2014) and reduced gray matter volume (Raji et al., 2012; Wang et al., 2014b; Wen et al., 2006) have been associated with increased volume of WMH. WMH may thus be a localized expression of widespread changes in both white and gray matter not detectable on clinical brain MRI examination and reading. Localization of volumetric and diffusion changes at the whole brain level may provide novel clues to the pathological processes involved in WMH and increased understanding of the clinical manifestations associated with WMH.

Most previous studies have only examined the association between WMH and a single imaging metric, such as DTI-derived microstructural indices (van Leijsen et al., 2018; Leritz et al., 2014; Maillard et al., 2014; Vernooij et al., 2008), brain volume (Arvanitakis et al., 2016; Raji et al., 2012; Wen et al., 2006) or cortical thickness (Dickie et al., 2016a; Tuladhar et al., 2014). Hence, the concurrent effect of WMH on multiple image metrics, such as white matter microstructure and brain volumes, at the whole brain level remains largely unknown. In addition, the dominant use of regression between WMH load and imaging metrics, usually including those with no WMH, may not be optimal for uncovering all WMH-related brain changes such as differentiating between pathology related to presence of WMH and that associated with increasing WMH load. If WMH represent only one part of a widespread WMH-related brain pathology, presence of WMH per se may cause structural and/or microstructural alterations not necessarily sensitive to WMH load. Moreover, uncovering the regional changes in FA and MD with increasing WMH load has implications for our understanding of WMH and its impact on the brain. Although the regional effect of WMH load on FA and MD has been demonstrated (Leritz et al., 2014), the relative regional change in FA and MD to increasing WMH load is not known. Finally, studies of WMH have been performed predominantly in older people (>65 years) from hospital samples (Gouw et al., 2006; Tuladhar et al., 2014; van der Veen et al., 2014) or in selected, non-validated general populations (Dickie et al., 2016b; Jeerakathil et al., 2004; Verhaaren et al., 2011), making it difficult to generalize the findings to the general population and to middle-aged individuals in particular, which is the age when WMHs are considered to emerge (de Leeuw et al., 2001; Hopkins et al., 2006).

The primary goal of this study was to document the concurrent effect of WMH on white matter microstructure using the DTI indices FA and MD and whole brain regional volumes using tensor-based morphometry (TBM). We examined regional differences in white matter microstructure and brain volumes between people with and without WMH. The group comparisons aimed at revealing changes due to the presence of WMH per se. To further substantiate if mere presence of WMH has widespread effects on the brain, we examined group differences in microstructure and brain volumes between people with age appropriate WMH (i.e. Fazekas grade 1) (Inzitari et al., 2007) and people without WMH. We then investigated the associations between WMH load and white matter

microstructure and brain volumes within the WMH group to elucidate brain changes that co-varied with WMH load. Lastly, we investigated patterns of FA and MD changes to increasing WMH load in the WMH group to identify possible presence of heterogeneity in white matter microstructural changes.

2. Materials and methods

This study was approved by the Regional Committee for Ethics in Medical Research (REK-Midt #2011/456) and the HUNT board of directors. All participants gave written informed consent before participation.

2.1. Participants

The participants were drawn from the Nord-Trøndelag Health Surveys (HUNT) study. The HUNT study is a collaboration between the HUNT Research Centre (Faculty of Medicine, Norwegian University of Science and Technology), the Nord-Trøndelag County Council, the Central Norway Health Authority and the Norwegian Institute of Public Health. HUNT is a multipurpose general population survey in which the entire population older than 12 years of age in Nord-Trøndelag County, Norway, can participate. As a follow up to HUNT3, a group of 1006 individuals between age 50 and 65 was invited to participate in a brain MRI study. Inclusion criteria were previous participation in HUNT1 (1984–86), HUNT2 (1995–97) and HUNT3 (2007–2009), and living less than 45 min by car or public transport from Levanger hospital where scanning was performed. Exclusion criteria were limited to standard MRI safety measures and weight above 150 kg. Approximate participation rates for the cohort aged 50–65 in HUNT3 were 90% in HUNT1, 80% in HUNT2 and 70% in HUNT3 (http://www.ntnu.edu/hunt/participation). Of those invited to HUNT-MRI, 27% declined participation, including those with MRI contraindications. Those who agreed to participate had an overall similar health status to both the declining and non-invited participants, but were less likely to be obese and hypertensive (Honningsvåg et al., 2012). None of the HUNT-MRI participants have been diagnosed with mild cognitive impairment (MCI) or AD based on hospital and dementia registry records.

2.2. Demographic data, clinical and blood measurements

Demographic data, clinical and blood measurements were obtained from HUNT3. Demographic data included age, education (1: primary school, 2: high school, 3: university/college), smoking history (pack-years, PY, i.e., the number of years with daily consumption of a 20-pack with cigarettes). Clinical data included diagnosis of diabetes, systolic blood pressure, resting heart rate, waist-hip-ratio and body mass index (Holmen et al., 2003; Krokstad et al., 2013). Non-fasting blood samples were drawn from participants and analyzed for total cholesterol, high-density lipoprotein cholesterol, glucose, triglycerides, and high sensitivity C-reactive protein (Bjerkeset et al., 2011; Chau et al., 2014). Evidence shows that both non-fasting triglyceride and non-fasting glucose levels predict cardiovascular events pointing to their clinical relevance (Bansal et al., 2007; Ferreira et al., 2017).

2.3. Image acquisition

All participates were scanned at Levanger Hospital, Nord-Trøndelag with the same a 1.5T Signa HDx MRI scanner (GE Healthcare, Milwaukee, Wisconsin, US) equipped with an 8-channel head coil. The same protocol was used throughout the study. We used sagittal T1-weighted, FLAIR and DTI images in this study. See Table 1 for scan sequence parameters. The scan protocol also included T2-weighted, T2*-weighted, and time-of-flight angiography scans not used in the present study. Full specifications of the scan protocol were described previously (Håberg et al., 2016).

Table 1
MRI scan parameters.

MRI sequence	Reconstructed matrix	TR (ms)	TE (ms)	Flip angle (deg)	Slice thickness (mm)	Number of slices/sections	Gap (mm)	FOV (mm)	Other
T1W (IR-FSPGR)	256×256	10.2	4.1	$10°$	1.2	166	0	240	
FLAIR	256×256	11002	122.9	$90°$	4.0	27	1	230	axial 2D
DTI (SE-EPI)	256×256	13500	104.6	$90°$	2.5	60	0	240	axial, 40 directions with b = 1000 s/mm^2 and 5 images with b = 0 s/mm^2
T2W	512×320	7840	95.3	$90°$	4.0	27	1	230	axial 2D

Notes: W = weighted, IR-FSPGR = inversion recovery prepared fast spoiled gradient recalled sequence, FLAIR = fluid attenuated inversion recovery, SE-EPI = spin-echo planar imaging, FOV = field of view, TR = repetition time, TE = echo time.

2.4. Visual rating, manual delineation and creation of WMH maps

Fig. 1 provides an overview of WMH grading, stratification into groups, and subsequent analyses. First, semi-quantitative WMH rating was performed by consensus by two experienced senior consultant neuroradiologists based on a modified Fazekas score classifying the lesions into grade 0–3 (Fazekas et al., 1987; Inzitari et al., 2009, 2007). Fazekas grade 0 is given when WMH are deemed not present, Fazekas grade 1 describes WMH in the shape of caps and/or a thin lining around the lateral ventricles and/or punctate foci in deep gray matter. Fazekas grade 2 describes WMH that create a smooth halo around the ventricles and either larger or starting confluent foci in deep white matter while Fazekas grade 3 represents irregular periventricular signal extending into deep white matter and/or confluent WMH foci in deep white matter. Fazekas grade 1 is considered age appropriate in this age group, while grades 2 and 3 are considered excessive in this age group (Inzitari et al., 2007). Participants were stratified into a group having WMH, i.e. all with Fazekas grade ≥ 1, i.e. WMH group, and not having WMH, no-WMH group. To examine the effect of age appropriate WMH on white matter microstructure and brain volumes, participants were stratified into Fazekas grade 1 versus no-WMH group.

In the group with WMH, the WMH were delineated manually on the FLAIR images by a single trained research assistant, taking into account the T2 weighted images, using the Multi-image Analysis Graphical User Interface (MANGO, http://ric.uthscsa.edu/mango/mango.html)

software. The WMH were traced on each transverse slice. The T2W scan was used in cases where WMH foci could not be reliably determined on the FLAIR scan due FLAIR's lower lesion to brain tissue contrast, particularly in deep (and ventral) white matter, and susceptibility to flow and other artifacts at the base of the brain compared to T2W scans. Although automated methods for WMH compare well, but not excellent to manual delineation (Dadar et al., 2017), manual delineation is considered the gold standard and was chosen since the number of participants allowed for manual tracing. The intra-rater reliability of the manual delineation was assessed by tracing WMH lesions twice on 40 randomly selected images, giving an interclass correlation coefficient (ICC3) of 0.95. A spatial map of the lesions and the total WMH volume were obtained from the manual delineation. For those with Fazekas 0, WMH volume was set to zero.

In the WMH group, the WMH volume distribution had a positive skew (for WMH > 0: skewness = 5.37, kurtosis = 37.99). A "WMH load" parameter was calculated as the natural logarithm of the ratio between WMH and intracranial volume (ICV) to bring the data closer to a normal distribution and remove the dependency between WMH volume and gross brain volume. This WMH load parameter had skewness = 0.83 and kurtosis = 3.84 for the non-zero values. The ICV was calculated by inverse transforming a manually delineated ICV mask in template space as described by Hansen and co-workers (Hansen et al., 2015). A map of the spatial distribution of WMH was made by warping the WMH maps for each participant in the WMH group to template space using
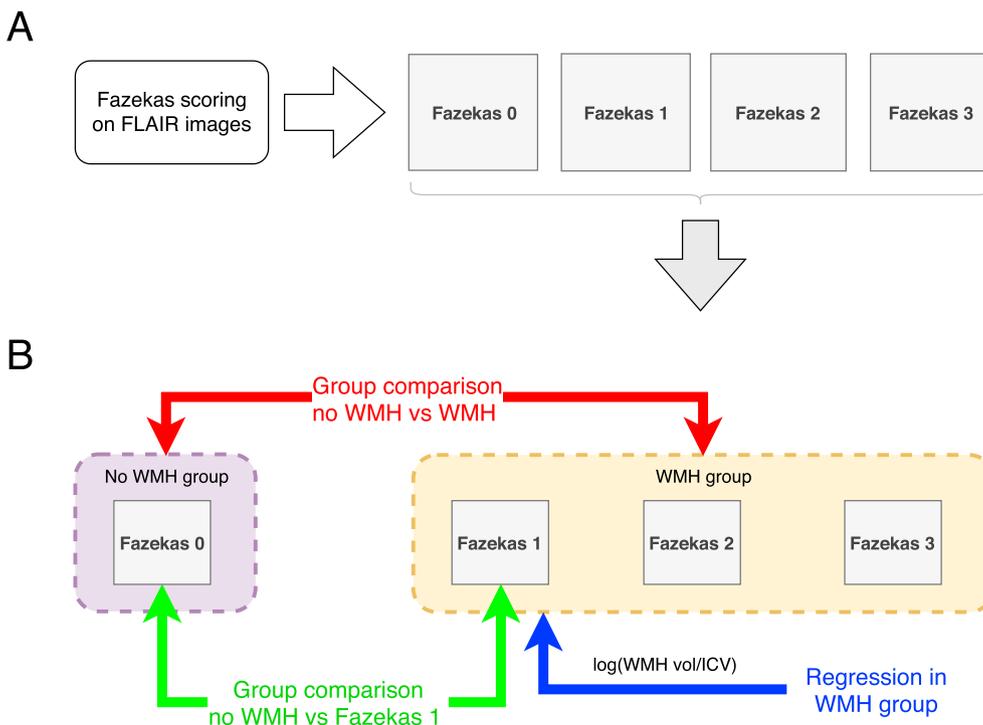

Fig. 1. Illustration of study design. A) Participants were rated with the Fazekas scale from the FLAIR images. B) Illustration of the three different statistical models used in the study. The no WMH group were those with Fazekas score 0, and the WMH group, those with Fazekas score ≥ 1. The red line signifies group comparison between the no WMH group and the WMH group. The blue line signifies regression on WMH load in the WMH group, and green line signifies the group comparison between the no WMH group and those with Fazekas 1.

nearest-neighbor interpolation. The warped WMH maps were added together and the resulting image divided by the total number of subjects, i.e. both those in the WMH and no-WMH groups (See Fig. 2 and the section on Image Processing for further details on template formation and image warping.). The distribution of WMH volume relative to Fazekas scores, the WMH volume distribution for each sex and the regression between age and WHM volume (for the WMH group) were plotted for visualization purposes.

2.5. Image processing

The image processing pipeline is illustrated in Fig. 2. For each participant, the FLAIR images, WMH maps, and DTI images were co-registered, but not resliced to the T1W image using SPM12 (http://www.fil.ion.ucl.ac.uk/spm/). Specifically, the FLAIR image was rigid-body registered to the T1W image, and the transform applied to register the manual WMH delineation. Similarly, for the DTI data, the

first $b = 0$ s/mm^2 image was rigid-body registered to the T1W image, and the transformation was applied to the other diffusion images. Next, T1W images were segmented using SPM12 with default options. A brain mask for skull-stripping the T1W images were constructed by thresholding the three tissue probability maps (gray matter, white matter, and cerebrospinal fluid) at $p > 0.05$ and combining the three masks, ensuring a 95% probability that the brain mask belongs to either gray matter, white matter or cerebrospinal fluid. The skull stripped T1W images were corrected for intensity inhomogeneities using the N4 bias field correction algorithm (Tustison et al., 2010). DTI images were corrected for motion and eddy currents, the diffusion vectors adjusted to account for the motion correction, and diffusion tensor indices (FA and MD) were computed with weighted least squares regression using the FSL program package (http://www.fmrib.ox.ac.uk/fsl, version 5.0.9).

A study-specific T1W template was made with the ANTS toolkit (http://stnava.github.io/ANTs/, version 2.1.0). The template was created from 32 T1W images with Fazekas grade 0. They were selected by

Fig. 2. Flow chart of the image-processing pipeline showing the data transformations of each image modality. Rectangles indicate images, parallelograms computations, solid arrows transfer of image data, and dotted lines images used as reference for registration or non-linear warping.

dividing the data into four age groups, 50–54, 55–59, 60–64 and 65–66 years, and randomly selecting four men and four women in each age group. Selecting evenly from each age group avoided biasing the template to any specific age range. The study-specific template was generated with the "antsMultivariateTemplateConstruction" script using the 32 skull stripped T1W images. The T1W template was resampled to 1.5 mm isotropic resolution to reduce memory requirements for the voxel-wise statistics (described below).

WMH appear hypointense on T1W images, which may affect the non-linear normalization, as shown for multiple sclerosis lesions (Sdika and Pelletier, 2009). To avoid spurious effects of WMH on the T1W normalization, we used a lesion-filling method in FSL to mask white matter hypointense regions with intensities similar to normal-appearing white matter (Battaglini et al., 2012). Due to the large slice thickness of the FLAIR images, optimal results were achieved by merging the manually drawn WMH mask with the T1W-hypointensity labels from Free-Surfer (FreeSurfer data used in (Hibar et al., 2017)). The resulting "T1W-hypointense" mask was used in the lesion-filling script to mask hypointense white matter regions in the T1W images. The skull stripped and lesion-filled T1W images were warped to the study-specific template with the "antsRegistration" program in ANTS using the symmetric image normalization (SyN) transform (Avants et al., 2008) with a cross-correlation metric.

FA and MD images from the fit of the diffusion tensor model were normalized to the template by a two-step procedure that avoids logical circularity in the registration (Tustison et al., 2014). A nonlinear transform was computed for the warp between the first non-diffusion weighted image and the subject's native T1W image using a SyN transform and a mutual information cost function. The DTI indices were subsequently warped to the template by combining the "DTI-to-T1W" and "T1W-to-template" warps. Prior to statistical analysis the FA and MD images were smoothed with a $\sigma = 2$ mm Gaussian kernel.

The Jacobian matrix of the nonlinear transform to template space was used to assess regional volume differences using TBM (Ashburner and Friston, 2004). The determinant of the Jacobian matrix describes the voxel-wise volume expansion or contraction required to match the template. ANTS uses only the non-linear transform in computing the Jacobian, not the affine part, making it unnecessary to account for gross head size when statistically comparing the Jacobian maps. The Jacobian determinant, however, is not well suited for statistical analysis since it is asymmetric with respect to volume expansion and contraction, and has a skewed distribution. The logarithm of the Jacobian determinant brings the data closer to a normal distribution and symmetrize the data around zero so that volume contractions have negative values, and volume expansions positive values (Leow et al., 2007). Therefore, the smoothed logarithm of the Jacobian determinant ($\sigma = 2$ mm Gaussian kernel) was used in the statistical analyses of volume changes. For brevity, we refer to the analysis of the log-Jacobian images as volumetric analysis henceforth.

2.6. Statistical analysis

Demographic and clinical data were compared between those included and excluded from the study, as well as between no-WMH and WMH groups using the R software for statistical computing, version 3.4.0 (R Core Team, 2017) with the "dplyr", "boot" and "VGAM" packages (Canty and Ripley, 2017; Wickham, 2011; Yee, 2010).

For all participants, the association of WMH load by age, sex, and clinical risk factors were examined with a Tobit multivariate regression model treating the zero WMH volumes as censored measurements (Yee, 2010). We selected risk factors available in the HUNT3 study previously associated with WMH: age and sex (Nyquist et al., 2015), BMI (King et al., 2014), blood glucose levels (Cherbuin et al., 2015), smoking history in packs per year (van Dijk et al., 2008), systolic blood pressure (van Dijk et al., 2008), cholesterol to high-density lipoprotein ratio (Dickie et al., 2016b), education (Habes et al., 2016) and C-reactive protein (CRP)

levels (Dufouil et al., 2012). Participants with high sensitivity C-reactive protein values > 10 were excluded from the analyses of risk factors to assess low-grade inflammation only (Bjerkeset et al., 2011).

We tested for the effect of the presence of WMH by comparing the WMH group (Fazekas grade ≥ 1) and the no-WMH group (Fazekas grade = 0) with regard to brain volumetric, FA and MD maps. An ANCOVA model with age and sex as confounders were used for all three analyses (volumetric, FA and MD). In the WMH group, the effect of WMH load on volumetrics, FA, and MD was investigated using multivariate regression with age and sex as confounding variables. Since more women had excessive WMH in the HUNT3 data (Håberg et al., 2016), we examined whether the regression slopes for males and females were different with an interaction term between sex and WMH load in the WMH group. To assess whether previously identified WMH risk factors (see above) affected the statistical analysis of volume, FA, and MD, we repeated the analyses above with age, sex, BMI, blood glucose levels, smoking history in packs per year, systolic blood pressure, cholesterol to high-density lipoprotein ratio, CRP, and education as covariates. Finally, we examined the effect of age appropriate WMH, i.e. Fazekas grade 1 (Inzitari et al., 2007), versus no WMH, on brain volumetrics, FA and MD.

Statistical inference on image data was performed using a non-parametric permutation-based inference method implemented in PALM version alpha-1.05 (Winkler et al., 2014). To speed up the calculations, we used the tail approximation with 1000 permutations, which has a negligible impact on accuracy (Winkler et al., 2016). The threshold-free cluster enhancement method (Smith and Nichols, 2009) were used for multiple comparison correction in all analyses. A family-wise corrected $p < 0.05$ was considered significant. For analysis of the volumetric data, we used a mask covering the whole brain, brainstem, cerebellum and ventricles. For the DTI data, a mask was generated by including all voxels with FA > 0.1 for all subjects' FA maps in template space. This latter mask included most cerebral and cerebellar white matter except peripheral regions bordering cortical gray matter (Supplementary Fig. 1). A threshold of FA > 0.1 was chosen to ensure that WMH were included in the mask. The statistical maps were finally warped to MNI space for visualization and to aid identification of brain regions using atlases in the FSL program package. In particular, the Johns Hopkins University white matter atlas (Hua et al., 2008) was used to identify the location of white matter tracts, while the thalamic connectivity atlas (Behrens et al., 2003) was used to identify cortical projections from thalamic regions. The warp used to bring the statistical maps to MNI space was obtained from an ANTS SyN transform of the study-specific T1W-template to the MNI T1W-template supplied with FSL. The study-specific T1W template was used as an underlay for the volumetric results, and the mean of all FA images for the DTI results.

The relative strengths of the associations between WMH load and FA and MD were assessed by extracting the standardized beta coefficient maps from the regression of WMH load on FA and MD with sex and age as covariates. The standardized beta coefficients were discretized into three bins: non-significant, small change and large change for FA and MD, respectively. The two latter bin sizes were determined by splitting the pooled beta values at the 5% trimmed mean. Each combination of the discretized data for FA and MD, i.e. non-significant FA and low MD, non-significant FA and high MD etc., eight in total, since the regions with non-significant changes in both FA and MD were omitted, was given a unique color and plotted voxel-wise to identify spatial patterns in the sensitivity of FA and MD to changes in WMH load.

3. Results

Of the 1006 subjects that underwent MRI scanning, 133 were excluded due to pathology, image artifacts or missing data (Fig. 3), resulting in 873 participants with useable T1W images, and 803 with high-quality DTI scans. The excluded subjects were on average one year older, had higher BMI, higher waist-hip-ratio and higher prevalence of diabetes than those included (see Supplementary Table 1). Key
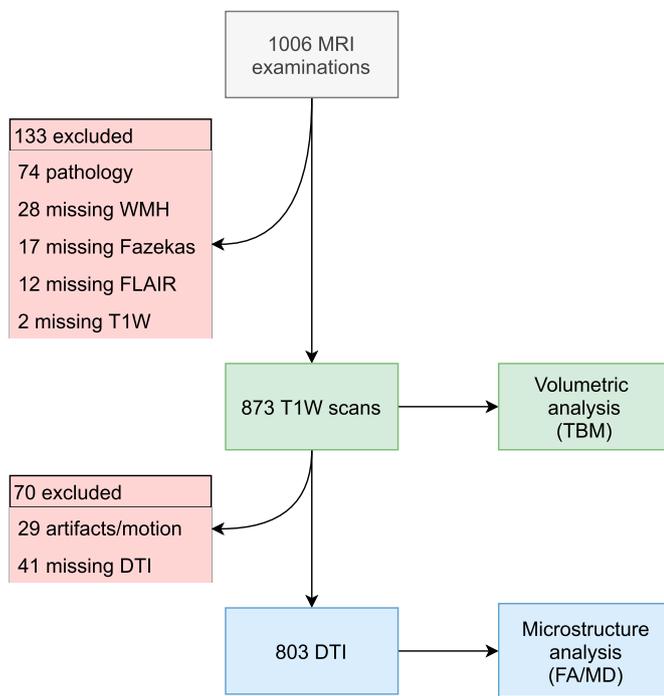
Fig. 3. Flow chart depicting the reasons for exclusion of subjects from the volumetric and DTI analyses.

demographic and somatic characteristics of the included participants are reported in Table 2 and Supplementary Table 2 for the participants in the DTI analyses. The no-WMH and WMH groups did not differ significantly on most variables in Table 2, but the WMH group was significantly older (1.6 years) and contained more women (57%). For the participants in the DTI analysis (Supplementary Table 2), only age was significantly different between the no-WMH and WMH groups.

Of the 873 included participants in the volumetric analysis, there were 476 (54.5%) with no WMH, 324 (37.1%) with Fazekas grade 1, 60 (6.8%) with Fazekas grade 2, and 13 (1.5%) with Fazekas grade 3. The distribution was similar for the DTI dataset. (See Table 3 for a summary of number of subjects and WMH volume for each Fazekas grade for both the volumetric and DTI datasets.) Thus the majority had age appropriate WMH, and only a minority excessive WMH. The box-plot in Fig. 4A shows the mean and variance in WMH volume for each Fazekas score. There was a slight excess of women with WMH: 57% with Fazekas 1, 53% with Fazekas 2 and 78% with Fazekas 3 (Fig. 4B). There was a significant linear association between age and WMH load in the WMH group (Fig. 4C) (r = 0.21, p = 2e-5, 95% CI [0.12, 0.30]). The WMH frequency map based on the entire sample (Fig. 4D) showed that WMH occurred most frequently as caps around the anterior and posterior horns of the lateral ventricles and to a lesser extent lining the lateral aspect of the lateral ventricles. The regions with the second most frequent locations were deep white matter in the frontal lobes.

3.1. Associations between WMH load and risk factors across entire sample

Multivariable regression with WMH load as dependent variable and explanatory variables age, sex and WMH risk factors showed that age, sex, smoking in pack-years and systolic blood pressure were significantly associated with higher WMH load (Table 4). Despite several significant factors, the model explained only 8.8%, 95% CI [6.1%–13.8%] of the variance in the WMH load variable.

3.2. Differences in brain volume between WMH and no-WMH groups

Voxel-wise group comparison of the volumetric data revealed regions

Table 2
Demographic and somatic characteristics of all subjects in the volumetric analysis and for the no-WMH and WMH groups separately.

	All (N = 873)	no WMH (N = 476)	WMH (N = 397)	p-value (t or χ^2)
Age	58.8 ± 4.2 (58.5–59.1)	58.1 ± 4.2 (57.7–58.5)	59.7 ± 4.0 (59.3–60.1)	<0.0001*
Females	464 (53.2%)	238 (50.0%)	226 (56.9%)	0.05*
Education[a]	1.86 ± 0.71 (1.82–1.91)	1.86 ± 0.70 (1.80–1.92)	1.87 ± 0.73 (1.79–1.94)	0.97
WMH volume (ml)[b]	–	–	0.9 (0.5–1.7)	–
BMI (kg/m2)	26.8 ± 3.7 (26.6–27.1)	26.7 ± 3.5 (26.4–27.1)	26.9 ± 3.9 (26.6–27.3)	0.63
Waist hip ratio	0.90 ± 0.07 (0.90–0.90)	0.90 ± 0.07 (0.89–0.91)	0.90 ± 0.07 (0.89–0.91)	0.95
Cholesterol-HDL ratio	4.4 ± 1.3 (4.3–4.5)	4.5 ± 1.3 (4.4–4.6)	4.4 ± 1.3 (4.2–4.5)	0.10
Glucose (mmol/L)	5.59 ± 1.66 (5.48–5.71)	5.58 ± 1.73 (5.42–5.74)	5.60 ± 1.58 (5.44–5.76)	0.97
Diabetes	25 (2.9%)	11 (2.3%)	14 (3.5%)	0.31
SBP (mmHg)	131.6 ± 17.0 (130.5–132.8)	130.6 ± 16.1 (129.2–132.1)	132.8 ± 17.9 (131.1–134.6)	0.10
Hypertension	238 (27.3%)	117 (24.6%)	121 (30.5%)	0.06
Smoking[c]	213 (24.4%)	107 (22.5%)	106 (26.7%)	0.15
Pack years[d]	8.7 ± 11.6 (7.9–9.5)	8.3 ± 11.4 (7.2–9.3)	9.3 ± 11.8 (8.1–10.5)	0.21
CRP < 10 (mg/L)[e]	1.66 ± 1.65 (1.54–1.77)	1.65 ± 1.69 (1.50–1.81)	1.66 ± 1.60 (1.50–1.82)	0.53

Unless stated otherwise, values are given as mean ± standard deviation (95% confidence interval) for continuous variables and count (%) for dichotomous variables. Missing measurements (percentage relative to total): BMI 1 (0.1%), cholesterol-HDL ratio 45 (5.2%), glucose 45 (5.2%), SBP 4 (0.5%), smoking 14 (1.6%), pack-years 28 (3.2%), hypertension 4 (0.5%), CRP 4 (0.5%).
*Differences between no-WMH and WMH groups were calculated with t- and χ^2 tests, with p < 0.05 considered significant.
Abbreviations: High sensitivity C-reactive protein (CRP), high-density lipoprotein (HDL), body-mass-index (BMI), systolic blood pressure (SBP).
[a] Education coded as 1 = primary school, 2 = high school, 3 = university/college.
[b] Median (interquartile range).
[c] People smoking at the time of examination.
[d] Pack-years defined as number of cigarettes smoked per day multiplied by number of years smoking and divided by 20.
[e] 30 persons with CRP >10 and were excluded from the CRP results, but were not counted as missing.

Table 3
Number of subjects, mean and median WMH volume for each Fazekas rating for the dataset used in the volumetric and microstructural analyses.

Type of Analysis	Fazekas 0	Fazekas 1	Fazekas 2	Fazekas 3
Volumetric: N (%)	476 (54.5%)	324 (37.1%)	60 (6.8%)	13 (1.5%)
Microstructural: N (%)	431 (53.7%)	302 (37.6%)	58 (7.2%)	12 (1.5%)
Volumetric: WMH volume (ml)[a]		1.02 (0.74)	2.87 (2.91)	10.10 (6.38)
Microstructural: WMH volume (ml)[a]		1.03 (0.75)	2.81 (2.91)	9.31 (6.17)

[a] Mean volume with median volume in parenthesis.

with both increased and decreased volume in the WMH group compared to the no-WMH group as shown in Fig. 5 and Supplementary Fig. 2 for the corresponding effect size maps. The WMH group had larger volumes of the lateral ventricles, the head of caudate nucleus bilaterally and in a small region in the left insula. The largest effect sizes were in the head of the caudate nucleus bilaterally (Cohen's d 0.34–0.42). The WMH group had smaller volumes in the brainstem, cerebellar white matter, thalamus, splenium of the corpus callosum, and inferior temporal lobe (fusiform and inferior temporal gyrus). Here the largest effect sizes (Cohen's
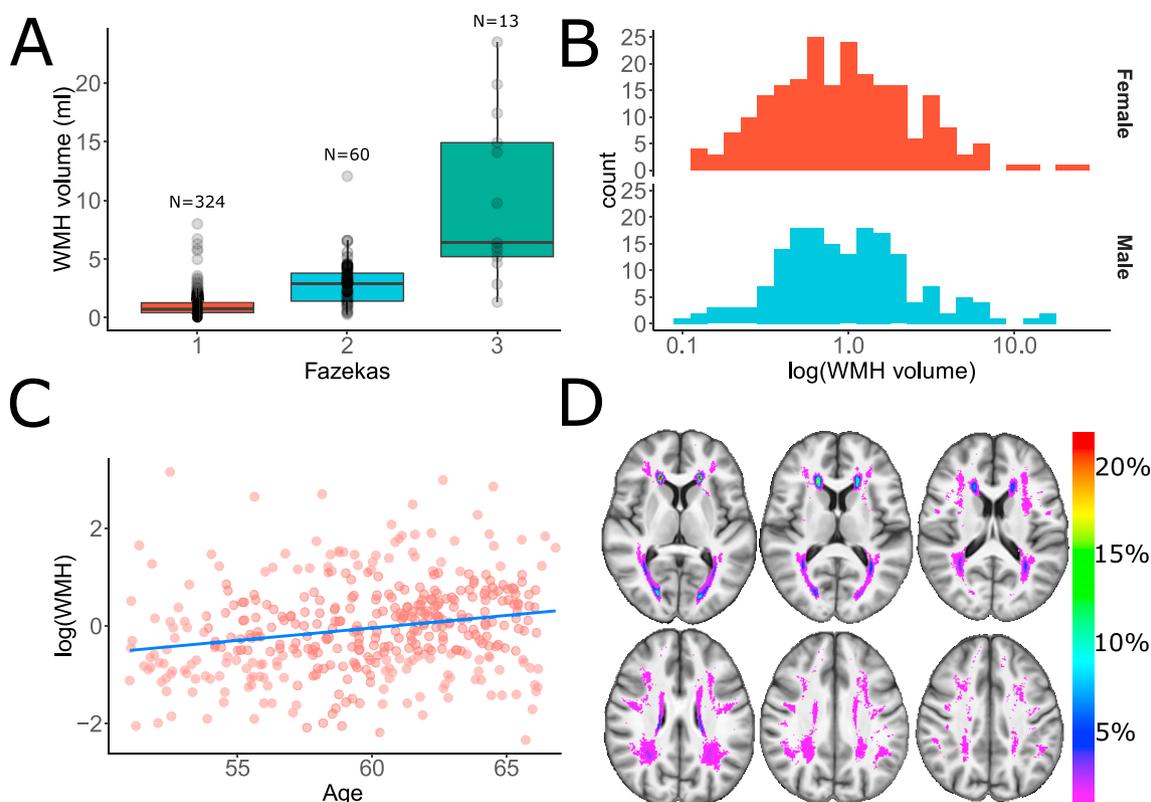
Fig. 4. Characterization of WMH lesions. (A) Manually delineated WMH volume versus Fazekas grade. Above each category are the number of subjects for each Fazekas grade in the volumetric analysis. (B) Distribution of WMH load for men and women for those in the WMH group (Fazekas ≥ 1). (C) Natural logarithm of WMH load versus age. Blue line is the linear fit to the data (r = 0.21, p = 2e-5). (D) Spatial frequency map of WMH lesions based on the manual delineation in the FLAIR images. Frequencies were calculated on the whole sample, i.e. both the WMH and no-WMH groups.

Table 4
Tobit regression of WMH load on potential risk factors (N = 786).

	Estimate	95% CI			p
Age (years)	0.109	0.075	–	0.143	0.000*
Sex male	−0.367	−0.659	–	−0.075	0.014*
Education level	0.041	−0.062	–	0.144	0.431
BMI (kg/m^2)	0.002	−0.040	–	0.043	0.940
Glucose (mmol/L)	−0.001	−0.084	–	0.082	0.984
Smoking (pack-years)	0.017	0.004	–	0.029	0.009*
SBP (mmHg)	0.010	0.002	–	0.019	0.019*
CRP< 10 (mg/L)	−0.078	−0.170	–	0.015	0.099
Cholesterol-HDL-Ratio	0.005	−0.120	–	0.130	0.937

[a]Education coded as 1 = primary school, 2 = high school, 3 = university/college.
[b]Only individuals with low-grad inflammation included; CRP< 10 (mg/L).
*p < 0.05 considered significant.
Abbreviations: High sensitivity C-reactive protein (CRP), high-density lipoprotein (HDL), body-mass-index (BMI), systolic blood pressure (SBP), confidence interval (CI).

d 0.26–0.35) were in the part of the right thalamus that projects to the primary motor and pre-motor areas, the brainstem, and the splenium of the corpus callosum. The inclusion of the WMH risk factors as confounders reduced the significance and extent of the difference, but the results were qualitatively similar to the analysis with only age and sex as co-variates (Supplementary Fig. 3). The analysis comparing the no-WMH group to the Fazekas grade 1 group, revealed decreased volume in the thalamus and brainstem, but no regions with significantly increased volume in the Fazekas grade 1 group (Supplementary Fig. 4).

3.3. Associations between brain volume and WMH load

The interaction between sex and WMH load was non-significant in the voxel-wise regression analysis, indicating that the association were the same for men and women. Positive associations between WMH load and brain volumes were found in the ventricles, caudate, posterior limb of the internal capsule and insula as shown in Fig. 6 and Supplementary Fig. 5 for the corresponding Pearson's correlation coefficient maps. The strongest correlations (r = 0.31–0.41) were around the anterior ventricular horns and head of the left caudate. Regions with a negative association between brain volume and WMH load included the left cerebellum stretching from I-IV to Crus I, cerebellar white matter, brainstem, thalamus bilaterally and in cortical and near-cortical regions in left precuneus, superior part of the central sulcus bilaterally and right supplementary motor area (Fig. 6). The strongest associations (r = 0.17–0.28) were in the superior part of the central sulcus bilaterally, right supplementary motor area, thalamic regions bilaterally projecting to the motor, premotor and posterior parietal cortices, cerebellar left VI and left VIIb (Supplementary Fig. 5). Similar to the group comparison, regression with additional WMH risk factors as confounders were qualitatively similar to the analysis without the risk factors (Supplementary Fig. 3). The lower volumes in the thalamus, however, were no longer significant when correcting for risk factors.

3.4. Differences in FA and MD due to presence of WMH

The WMH group had lower FA and higher MD in large parts of white matter compared to the non-WMH group (Fig. 7, and corresponding effect size maps in Supplementary Fig. 6). FA was reduced in the body of the corpus callosum, anterior limb of the internal capsule, posterior thalamic radiation, and parts of the superior longitudinal fasciculus, indicating that both inter- and intrahemispheric projections were affected. FA was also decreased in subcortical gray matter regions, including parts of the thalamus, caudate and posterior putamen
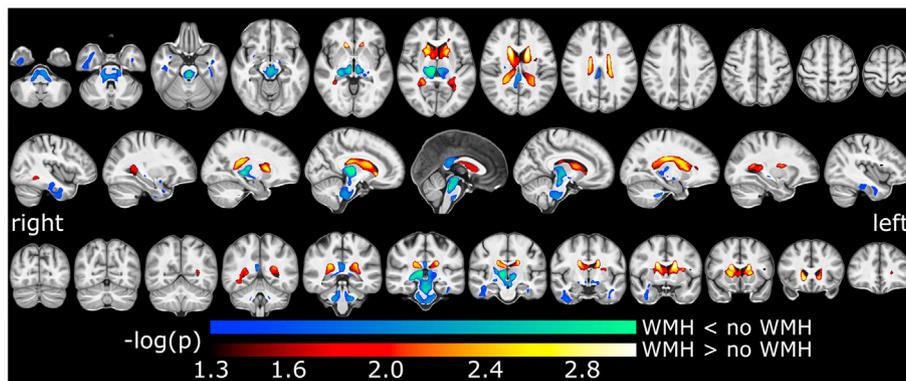
Fig. 5. Volume differences between WMH and no-WMH groups corrected for age and sex (p(FWE) < 0.05). Red – yellow colors signify greater volume in the WMH group. Blue – green colors signify greater volume in the no-WMH group. Results are overlaid the study-specific T1W-template.
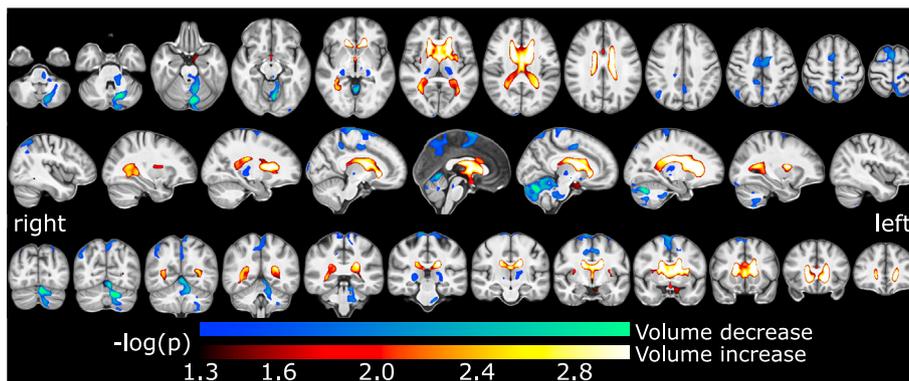

Fig. 6. Association between WMH load and regional volume for the WMH group, corrected for age and sex (p(FWE) < 0.05). Red – yellow colors indicate positive association with WMH load. Blue – green colors indicate negative association with WMH load. Results are overlaid the study-specific T1W-template.
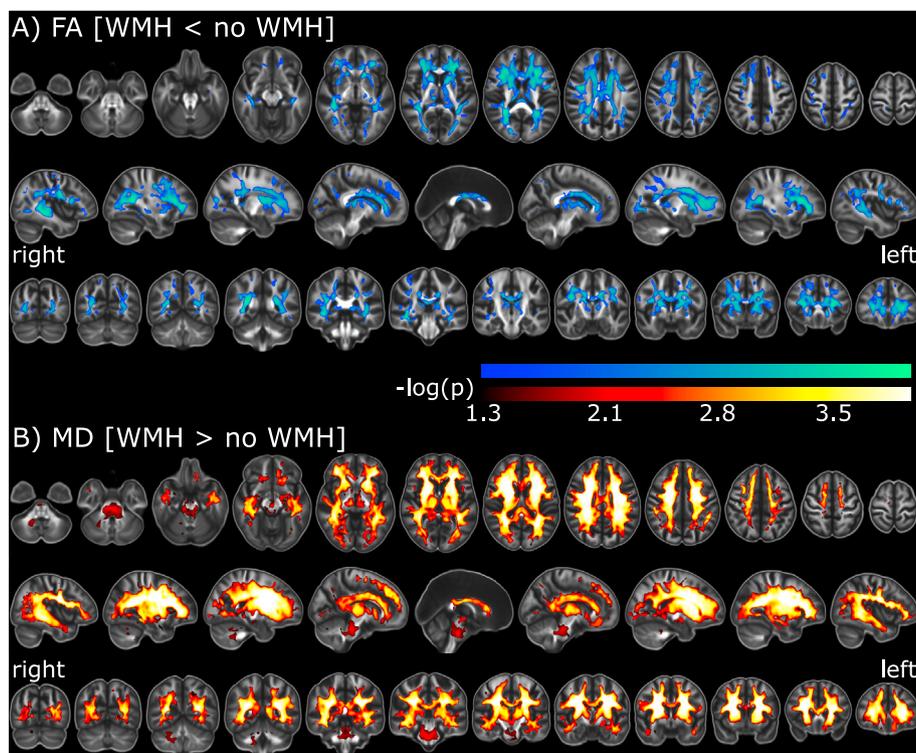
Fig. 7. Group differences in DTI indices between WMH and no-WMH groups corrected for age and sex (p(FWE) < 0.05). (A) Regions where FA was significantly decreased in the WMH group. (B) Regions where MD was significantly increased in the WMH group. Results are overlaid the mean FA image.

bilaterally. The largest effects for FA were in the right anterior limb of the internal capsule, near the posterior lateral ventricular horns bilaterally and deep frontal white matter bilaterally (Cohen's d 0.35–0.46). In the WMH group, MD was increased in most parts of white matter and subcortical gray matter (Fig. 7). The peak effect sizes for the MD differences were stronger and more extensive than for FA, but in the approximate same locations as for FA, i.e. in the right anterior limb of the internal capsule, posterior lateral ventricular horns and deep white matter in the frontal lobes (Cohen's d 0.48–0.72). The extent of significant group differences between the WMH and no-WMH group was greater for MD than FA, covering 61% of the analyzed volume, compared to 26% for FA. The inclusion of WMH risk factors as confounders had a negligible effect on the statistics (Supplementary Fig. 7).

The group comparison of DTI indices between Fazekas grade 1 and no-WMH groups revealed a similar pattern of differences in FA as in the WMH versus no-WMH group comparison (Supplementary Fig. 8). The regions were, however smaller and less significant than in the WMH versus no-WMH group comparison, in particular the group differences in the deep white matter and in white matter near the cortex were notably smaller in the Fazekas grade 1 and no-WMH comparison. The analysis for MD, on the other hand, was similar to the WMH versus no-WMH group, except for in the brainstem, where fewer significant group differences were uncovered (Supplementary Fig. 8).

3.5. Associations between DTI indices and WMH load

Regression between WMH load and DTI indices within the WMH group revealed a negative association with FA and a positive association with MD (Fig. 8 and corresponding Pearson's correlation coefficient maps in Supplementary Fig. 9). Similar to the volumetric analysis, the interaction between WMH load and sex was non-significant. Significant negative associations between WMH load and FA were found in the posterior limb of the internal capsule, part of the superior longitudinal fasciculus, parts of the inferior longitudinal fasciculus adjacent to the ventricles and regions close to the cortex in frontal and parietal lobes.

The largest correlation coefficients (Pearson's r 0.32–0.4) were approximately in the same regions as the peak Cohen's d values for the WMH versus no-WMH group differences. For the posterior ventricular horns, the overlap was almost perfect, but for the regions in deep frontal white matter, the loci were posterior to the loci with largest Cohen's d values. A significant positive association between WMH load and MD were present in white matter regions including the posterior limb of the internal capsule (mainly genu and body), the external capsule and deep white matter and in subcortical gray matter regions including the thalamus, putamen, and head of the caudate. The greatest correlation coefficients (Pearson's r 0.43–0.54) were approximately co-located with the maxima in the Cohen's d maps for the group differences in MD between the WMH and no-WMH groups, with maxima near the posterior ventricular horns, deep frontal white matter and right anterior limb of the internal capsule. The total volume of significant regions in the regression analyses were 33% for FA and 31% for MD. This is in contrast to the WMH versus no-WMH group comparison where the significant changes in MD covered a substantially greater volume than for FA. The inclusion of WMH risk factors in the regression model had a negligible impact on the results for both FA and MD (Supplementary Fig. 10).

3.6. Different patterns of change in FA and MD associated with WMH load

The partitioning of the standardized beta coefficients (Fig. 9) resulted in 76% of the data falling into three roughly equal-sized categories, dark blue (33%), light green (22%) and orange (21%). The dark blue category represented no change in MD and a small change in FA, and encompassed mainly white matter regions close to the cortex. The light green category represented a large change in MD and no change in FA. Tracts with these characteristics included the corticospinal tracts above the thalamus and parts of the superior longitudinal fasciculus. The orange category represented a large change in MD and a small change in FA. These regions were mainly located around clusters associated with a large change in MD and FA (red regions). The remaining 25% fell primarily into three smaller, roughly equal-sized categories, labeled dark green (9%), olive
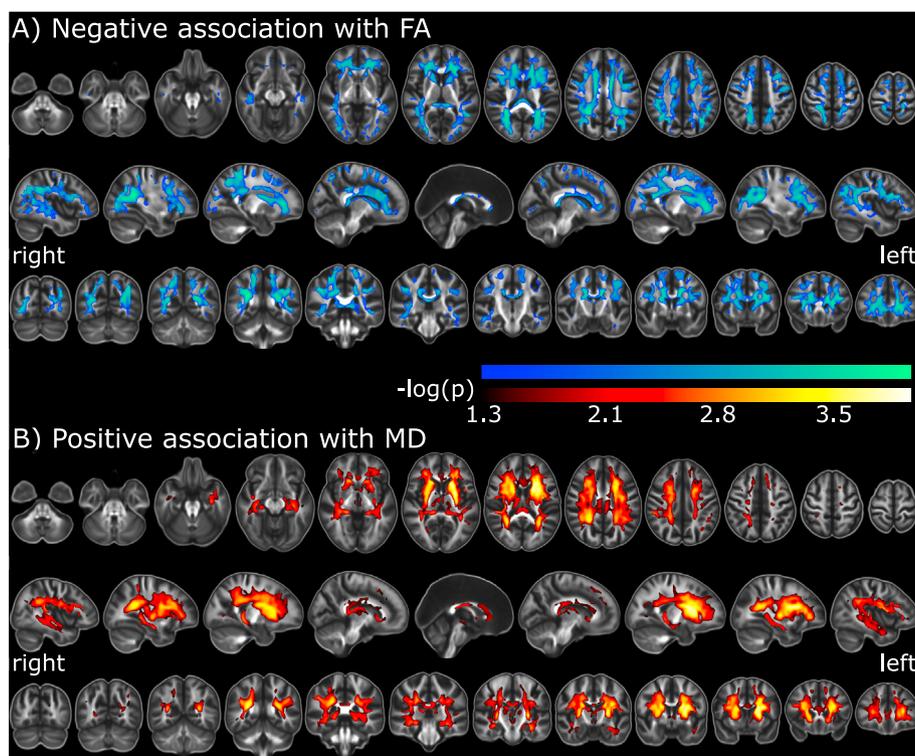
Fig. 8. Association between WMH load and DTI indices for the WMH group corrected for age and sex (p(FWE) < 0.05). (A) Regions with a significant negative association between WMH load and FA. (B) Regions with a significant positive association between WMH load and MD. Results are overlaid the mean FA image.
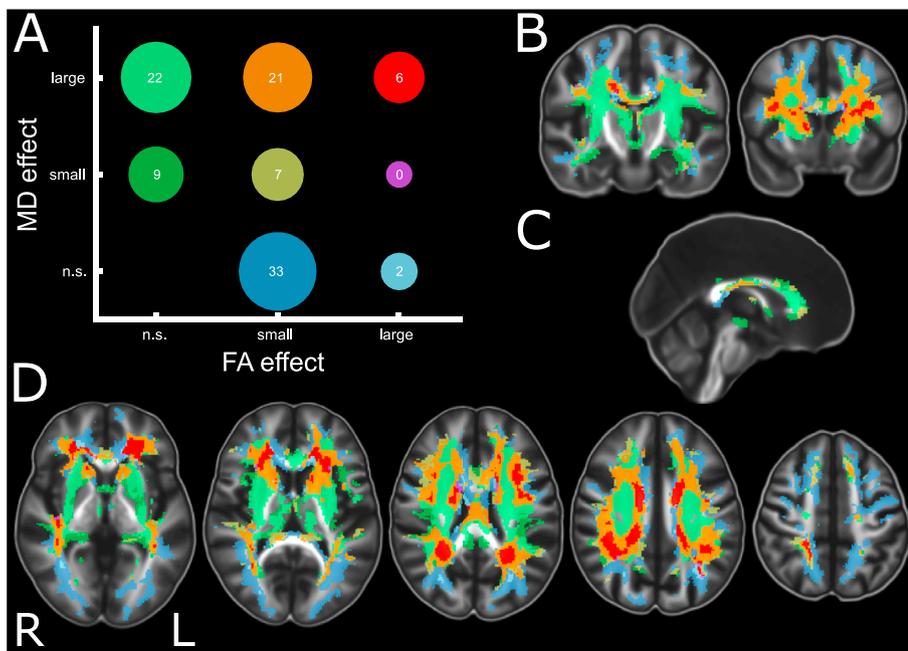
Fig. 9. The sensitivity of FA and MD to WMH load. (A) Distribution of standardized beta coefficients for the regression of FA and MD on WMH load. The coefficients are divided into three categories, non-significant effects (n.s.), "small" (<0.22) and "large" effects (≥0.22). Where 0.22 is the 5% trimmed mean of the pooled standardized beta coefficients from the FA and MD regression models. The numbers in each circle are percent volume relative to the volume of the regions with significant effects in FA and MD. Note that the size of the circles are not to scale. (B–D) Coronal, sagittal and axial sections showing the spatial distribution of the categories in (A) using the same color scheme as in the plot.

green (7%) and red (6%) in Fig. 8. There were no apparent patterns in the location of dark green and olive green regions, but the red regions, representing a large change in FA and MD, were in the caudate nucleus as well as in or adjacent to regions with a high frequency of WMH (see Supplementary Fig. 13).

3.7. The effects of presence of WMH versus the effect of increasing WMH load

For a qualitative comparison of the effect of presence of WMH to the effect of increasing WMH load, the statistical maps were color-coded with red signifying presence of both group differences and associations, blue signifying only group differences and green signifying only associations. See Supplementary Fig. 11 for the volumetric data and Supplementary Fig. 12 for FA and MD. There was a tendency for volume, FA and MD in regions in the brainstem and thalamus to be sensitive to the presence of WMH, whereas cortical and near cortical volume and white matter near the cortex were sensitive to increasing WMH load. There were also similarities in the results from the regression and group analyses for FA and MD. For MD, there were considerable similarities, with the exceptions of the pons and white matter regions near the cortex where only group differences were present. The FA results differed more markedly. FA differences in the thalamus and midsection of the corpus callosum were only present in the group comparison, while the regression analysis in the WMH group demonstrated significant associations primarily in white matter regions near the cortex. For brain volumes, there was almost no overlap between regions with a negative association in the regression analysis and regions with smaller volumes in WMH group compared to the no-WMH group (Supplementary Fig. 11B).

4. Discussion

This study was based on a large, validated, representative, healthy (Table 2 and Supplementary Table 2), community-dwelling general population sample of middle-aged participants between 50 and 66 years of age scanned on a single scanner with an identical scan protocol (Håberg et al., 2016; Honningsvåg et al., 2012). The narrow age range minimized age effects, and manual segmentation ensured accurate quantification of WMH. Our study was based on a younger cohort with lower WMH load than in comparable hospital and population studies

(Ikram et al., 2008; Jeerakathil et al., 2004; Wen et al., 2006). Due to the younger age of our sample, most subjects with WMH fell into the lowest WMH category, i.e., Fazekas grade 1, which is considered age appropriate WMH. Still, the frequency map of the spatial distribution of WMH was similar to those reported previously (de Laat et al., 2011; Habes et al., 2016; Rostrup et al., 2012), indicating consistent spatial predilection of WMH. Likewise, the WMH volume was clearly related to Fazekas grade (Fig. 4A), demonstrating that semi-quantitative scoring is a valid proxy for WMH load which can be applied both in both the clinic and research (Gouw et al., 2006).

Clinical risk factors previously identified as associated with WMH, including sex and age (Dickie et al., 2016b; Jeerakathil et al., 2004; Nyquist et al., 2015; van den Heuvel et al., 2004; van Dijk et al., 2008) explained at most 14% of the WMH load. The low explanatory power of known WMH risk factors has also previously been noted (Wardlaw et al., 2014). The sex effect on WMH has been speculated to emerge due to survival bias (Nyquist et al., 2015), but the current study does not support this notion as it was performed in middle-aged adults. The lack of significant interactions between sex and WMH load provides further support for WMH being driven by similar mechanisms in men and women, but with women on average having higher WMH loads for unknown reasons. Furthermore, adding risk factors as covariates to the analyses had minimal impact on the quantitative volumetry and DTI results in our sample. Indeed, the WMH and no-WMH groups were remarkably similar in demographic, somatic and psychiatric characteristics (Table 2 and Supplementary Table 2). Taken together, the origin of WMH remains elusive and appears to be governed mainly by factors we are unable to account for. Unaccounted factors could be cortical tau pathology (McAleese et al., 2015), cerebral amyloid levels (Scott et al., 2016) and blood-brain barrier integrity loss (Wardlaw et al., 2017) as suggested in recent studies. This study does, however, demonstrate that the effect of WMH is extensive encompassing both white and gray matter, with unique as well as common effect of presence of WMH and WMH load. Importantly, WMH of any grade was shown to significantly impact on the brain's macro- and microstructure, thus, no "age appropriate WMH" appear to exist.

4.1. The effect of presence of WMH on brain volumetry

The volume loss in the WMH group compare to the non-WMH group was located primarily in deep and central cerebral gray and white matter

structures, the brain stem and cerebellum. This volume loss was accompanied by lateral ventricular dilation. Contrary to the general finding of smaller brain parenchymal volumes, the caudate nucleus was larger in the WMH group (this group difference was present also when performing the analysis with volumes from FreeSurfer analysis). Indeed, the largest effect of presence of WMH was observed in the head of the caudate nucleus. The larger caudate volume in the WMH group might be related the catechol-o-methyltransferase (COMT) polymorphisms, which are reported to be associated with caudate and WMH volumes (Hill et al., 2013; Liu et al., 2014). However, since caudate volumes were similar in the Fazekas grade 1 and the non-WMH group (Supplementary Fig. 4), genetics alone cannot explain the larger caudate.

Many of the regions with volumetric differences in this group of healthy adults with WMH have been associated with increased risk of dementia or Alzheimer's disease (Brickman et al., 2015; Lee et al., 2016), including increased caudate volume (Persson et al., 2018), smaller thalamic volume (de Jong et al., 2008), smaller diencephalon volumes (Lebedeva et al., 2017), smaller fusiform and inferior temporal gyri (Desikan et al., 2008; Parker et al., 2018; Schwarz et al., 2017) and larger lateral ventricles (Nestor et al., 2008). Taken together this demonstrates volumetric brain changes in people with WMH similar to the changes seen in dementia, strengthening the previously observed connections between WMH and aberrant volumetry patterns in dementia (Lee et al., 2016).

4.2. The effect of WMH load on brain volumetry

We found that WMH load was associated with cerebral and cerebellar cortical volumes, which was not observed in the WMH versus no-WMH group analysis, as well as associations in regions affected by WMH per se such as the caudate, thalamus, brain stem and ventricles. Previous population based studies have demonstrated volume reduction associated with WMH in broad regions: the cerebellum, cerebral cortex, and cerebral white matter (Hoogendam et al., 2012; Schmidt et al., 2005; Smith et al., 2015) consistent with our findings. However, this study extended previous results showing a more comprehensive and detailed picture of the volume alternations associated with WMH load.

Thus, gray matter was demonstrated to be differentially sensitive to the presence of WMH and to increasing WMH load with increasing load affecting the cerebrum and cerebellum in a centrifugal manner, while WMH per se affect primarily the deeper and more central structures. The WMH load effect most likely reflects Wallerian degradation in cortex due to increased involvement of axons projecting to and from cortex as WMH load increases and affects deeper white matter more extensively (McAleese et al., 2017; Wardlaw et al., 2015). The volume loss associated with increasing WMH load was present in key structures involved in motor and cognitive control, including the motor and premotor cortices, cerebellum, thalamus, and brainstem, offering new insight into the association between WMH and gait and cognitive impairments reported in community-dwelling and clinical samples (Au et al., 2006; Bolandzadeh et al., 2014; Pinter et al., 2017; Silbert et al., 2008; Smith et al., 2011; Willey et al., 2013). There was also an association between WMH load and precuneus volume, a region affected early in the course of Alzheimer's disease with neuronal loss and hypoperfusion (Jacobs et al., 2012; Love and Miners, 2016). Interesting, precuneus is considered a region where cerebrovascular and Alzheimer's disease converge on a path leading to dementia (Love and Miners, 2016).

4.3. The effect of presence of WMH on FA and MD

The WMH group had lower FA and higher MD in large parts of central white matter's intra- and inter-hemispheric tracts compared to the no-WMH group (Fig. 7, corresponding effect size maps in Supplementary Fig. 6). For FA, only the posterior limb of the internal capsule and splenium of the corpus callosum were not involved of the central tracts. There was also some sparing of the posterior internal capsule for group

differences in MD. The posterior limb of the internal capsule in particular, but also splenium of the corpus callosum have been reported to have a higher myelin water fraction than their anterior counterparts (Arshad et al., 2016). It can be speculated that this structural feature helps preserveaxonal myelination and hence FA at a level not different from that in the no-WMH group even though the higher MD value in the WMH compare to the no-WMH group demonstrated effects of WMH also in these parts of white matter. FA was not different between the WMH and no-WMH groups in the white matter of the gyri, but higher MD values were observed at the base of the gyri. In comparison with FA, significantly higher MD values were almost 3 times as extensive and with larger effect sizes. The MD increase could be described as a growing edge or penumbra extending white matter changes beyond the FA effect in the presence of WMH.

The largest effects for FA were in the right anterior limb of the internal capsule, near the posterior ventricular horns bilaterally providing evidence for a role of WMH in motor/gait impartments. Moreover, with only visual pathways being relative spared, the WMH group demonstrated widespread microstructural changes which could impair cortical-subcortical, intra- and inter-cortical connectivity and thus affect higher order cognition in people with WMH. Loss of connectivity is a brain structural feature also connected to Alzheimer's disease (Stricker et al., 2009).

In the WMH group, diffusion changes were observed in subcortical gray matter as well. Both lower FA and higher MD were present in thalamus as well as higher MD in all other subcortical nuclei. Lower FA and higher MD in thalamus are observed in two other conditions recognized by widespread white matter injury, i.e. premature birth with very low birth weight (Eikenes et al., 2011) and diffuse axonal injury in traumatic brain injury (Håberg et al., 2015). The more marked diffusion changes in thalamus could results from loss or myelination of the lamellar system of myelinated fibers separating the thalamic subnuclei, loss or changes in afferent or efferent axons of thalamus or Wallerian degradation due to WMH in the thalamic radiation. The lower FA and higher MD in thalamus are most likely due to changes in myelin. Supporting this notion, thalamus has a higher neuronal count but lower neuronal density than the caudate and putamen suggesting higher degree of connectivity (Kreczmanski et al., 2007). The higher MD values in the caudate and putamen indicate loss of microstructure in regions with high neuronal density and could imply for instance reduced cellular packing and/or loss of synapses.

The group differences in FA were less pronounced in the comparison between Fazekas grade 1 and the no-WMH group, but for MD the results for both white matter and subcortical gray matter nuclei were highly similar, except in some regions of the brainstem. Taken together, our group comparisons demonstrated that MD changes are extensive and an early event in the presence of WMH, as previously described in cross sectional (Maniega et al., 2015) and longitudinal (van Leijsen et al., 2018) ROI studies. Changes in subcortical gray matter nuclei microstructure in people with WMH of all severities suggest that also processing, not only connectivity, may be affected by WMH.

4.4. WMH load associated with FA and MD and their patterns of concomitant change

In the WMH group, WMH load was associated with increasingly lower FA and higher MD in regions where group differences were uncovered and for FA in tissues not affected in the group analysis. A striking negative effect of WMH load on FA was demonstrated in the cortical gyri across the cortical mantle, a region where no group differences were found. MD, on the other hand was barely associated with only WMH load (very few green voxels for MD in Supplementary Fig. 12). Thus, increasing WMH load did not merely decrease FA and increase MD. Instead, a complicated and heterogonous mixture of microstructural changes was revealed showing that the sensitivity to a unit increase in WMH load varies substantially across the brain and has anatomical

specificity (Fig. 9). These findings are in agreement with the well-known association between decreased FA and increased MD with WMH load from previous ROI based studies on population samples (Bastin et al., 2009; Maniega et al., 2015; Vernooij et al., 2009), but also extend the previous findings by showing with greater spatial detail the regions which were associated with WMH load, and the regional sensitivity of FA and MD to WMH load.

By examining patterns of FA and MD changes, the current study demonstrated a heterogeneous intermingled pattern of changes in FA and MD with three dominant patterns in the relative change of FA and MD to increasing WMH load (Fig. 9). The regional specificity and qualitative different patterns of these changes suggest distinctive associations between WMH load and tissue microstructure.

The first pattern, decrease in FA and increase in MD with increasing WMH load (the red and orange regions in Fig. 9) showed spatial association with WMH regions. In particular, the "hotspot" regions (red areas in Fig. 9) were overlapping or adjacent to regions with high WMH frequency (Supplementary Fig. 13). These hotspot regions were typically surrounded by a region of large MD change and small FA change (orange areas in Fig. 9). Longitudinal studies find that WMH affects surrounding tissue by proximity (de Groot et al., 2013; Maillard et al., 2013), consistent with this pattern (red and orange regions). A concordant FA decrease and MD increase have been associated with demyelination and axonal loss (Zhang et al., 2010) which is in agreement with histological studies of WMH (Fazekas et al., 1993; McAleese et al., 2017). Oxidative glial cell damage in white matter surrounding WMH (Al-Mashhadi et al., 2015) is also consistent with the observation of an affected region surrounding the WMH (orange areas in Fig. 9). The current study revealed for the first time that regions most sensitive to WMH load (i.e. red and orange hotspot regions in Fig. 9), not necessary aligns with the regions affected by presence of WMH (Supplementary Fig. 13). For instance, the anterior limb of the internal capsule bilaterally seemed to be particularly susceptible to increasing WMH load possibly because tracts projecting from the anterior limb of the internal capsule cross the regions with high WMH frequency surrounding the anterior ventricular horns. The presence of hotspots not in direct proximity to WMH provides evidence for anterograde degeneration of axons in superior and peripheral tracts and supports the idea that the overt WMH represent a limited part of a pervasive pathology.

The second pattern, defined by a large increase in MD with increasing WMH load (light green areas in Fig. 9), was mainly confined to the thalamus, basal ganglia, the external capsule and corticospinal tract above the thalamus. Since these regions were more distant from the location of WMH and only associated with an increase in MD, a different mechanism may be involved in these changes. The increased MD and unaffected FA signify an increase in the size of the diffusion tensor, but not its shape. This is consistent with increased interstitial or extracellular fluid (Vernooij et al., 2009). The physiological implication of isolated MD changes remains uncertain, but if these changes reflect a shift in increased interstitial or extracellular fluid, the changes may be reversible, as seen in patients with type C hepatic encephalopathy (Kale et al., 2006) that linked increased MD without a concomitant change in FA with reversible brain edema. The large green regions in Fig. 9 may as such represent areas at risk, which could potentially be normalized if WMH pathology was understood and treatable.

The third pattern (blue regions in Fig. 9), mainly seen in white matter near the cortex and in anterior corpus callosum, was characterized by a small decrease in FA and unaltered MD with increasing WMH load. A change only in FA is consistent with retrograde neuronal degeneration or Wallerian degeneration (Concha et al., 2006; Zhang et al., 2010). The location of this pattern in tracts leading to regions with cortical thinning (see Fig. 6) provides support for the presence of degeneration of cortical neurons, via anterograde, retrograde or transneuronal degeneration, as part of WMH pathology, in particular as a consequence of increasing WMH load.

In summary, increasing WMH load impacts white matter tracts in a complex manner with local and long-ranging effects. Although further experimental evidence is needed to understand the exact nature of these patterns of changes, the distinct patterns and their regional specificity suggest a more complicated association between WMH and white matter microstructure than has previously been demonstrated. Which of these patterns of MD and FA changes represent reversible or penumbral tissues remains to be determined.

4.5. Differences between presence of WMH and increased WMH load

As expected both similarities and differences in regions affected were uncovered in the comparison of the effect of presence of WMH to the effect of association with WMH load for all three image metrics, volume, FA and MD. Thus, some white and gray matter regions were only sensitive to the presence of WMH, some only to increasing WMH load, and some to both. Comparing the significant findings for volume, FA and MD revealed that volume changes seldom were accompanied by changes in microstructure and vice versa, except in the thalamus and brainstem, where group differences in volume and MD overlapped. Changes in these regions were also observed in the comparison between the Fazekas 1 group and no-WMH group, suggesting that these regions are affected in an early phase in the development of WMH. On the other hand, cortical and cerebellar cortex and white matter microstructure near the cortex were only sensitive to increasing WMH load. Hence, regions vulnerable to the presence of WMH appeared to be affected from an early stage in the development of WMH while the regions associated with increasing WMH load demonstrated a centrifugal involvement, with tissue involvement moving from deep central to cortical areas. Thus, limiting the growth of WMH may reduce WMH's negative impact on the brain. Further studies will be needed to understand the cause of these differences and find preventive measures.

4.6. Are WMH part of normal aging?

Even age appropriate WMH (Fazekas score 1) were associated with significant volume loss and microstructural differences, affecting large parts of cerebral white matter, thalamus, caudate nucleus and brainstem. In general, WMH affected in particular the brain's motor regions, with direct involvement of white matter due to WMH in regions with motor fibers, "penumbral effects" in surrounding normal appearing white matter, long ranging microstructural effects in tracts as they move beyond the location of the WMH towards gray matter in motor cortex or basal ganglia or thalamus, and morphometric and microstructural changes in motor cortex, premotor cortex, basal ganglia and thalamus, likely due to Wallerian degeneration. The motor system is considered robust and less affected in normal aging (Cox et al., 2016). Thus, the presence of WMH at any load cannot be considered part of healthy aging, at least not in middle-aged people. Since studies report that WMH are omnipresent in the oldest old (de Leeuw et al., 2001; Fernando and Ince, 2004), WMH may be an inevitable part of aging, but due to its extensive and widespread negative effects on the brain, measures aimed at delaying age of onset of WMH and further increase in WMH load should be actively sought. However, effective mechanisms to target to limit WMH remain elusive, also clearly shown in this study. In the current participants who were relatively young and healthy, there were limited demographic group differences between the WMH and no-WMH groups, and known risk factors explained very little of WMH load. As WMH were demonstrated to be a heterogeneous pathology encompassing brain regions outside the overt lesions, it is conceivable that any set of risk factors will have limited explanatory power for a simple summary measure such as WMH load.

Although several of the findings related to presence or load of WMH were in regions involved in Alzheimer's disease, it should be noted that neither presence of WMH nor WMH load affected hippocampus or medial temporal cortex volumes or microstructure. This finding concur with previous report that WMH increases dementia vulnerability as an independent or synergistic factor with neurodegenerative pathology.

4.7. Strengths and limitations

Some limitations of the study need to be emphasized. The cross-sectional design made it impossible to draw any conclusions in terms of causality. We were also unable to compare statistically the effect of WMH presence to WMH load due to high collinearity between WMH load and the grouping variable (i.e. no-WMH and WMH), and could therefore not dissociate the independent effect of load and presence. WMH were only delineated for subjects deemed to have neuroradiologically determined WMH (Fazekas ≥1), and therefore some subjects in the no-WMH group may have unspecific white matter hyperintense regions not classified as WMH. The 2D FLAIR acquisition with slices thickness of 4 mm may have excluded detection of small WMH lesions potentially reducing the accuracy of the lesion volume measurements. Inaccuracies may also arise from partial voluming with gray matter, white matter or CSF. Potential errors in WMH volume due to partial voluming with gray matter and CSF were examined by resampling the WMH delineations to T1W space and masking with gray matter and CSF mask constructed from the FreeSurfer segmentation. Although the corrected WMH volumes were reduced by 23% on average, the correlation with the original WMH volume was high (r = 0.99), suggesting that gray matter or CSF partial voluming should have a minimal impact on regression statistics. To confirm this, we ran two regression models (volume and MD) with WMH load computed from the corrected WMH estimates, which showed minor differences to the original statistics (data not shown). We also did not segment gray and white matter in the volumetric analysis, such that the volumetric differences found in cortical regions may be due to changes in gray matter or white matter near the cortex, or both. Note that it is not possible to relate changes in diffusion indices to cellular changes from DTI data alone because different cellular changes can give similar changes in diffusion indices. Also, a full brain mask was used in the volumetric analysis, while a smaller mask (Supplementary Fig. 1) was used in the DTI analyses, covering cerebral white matter, part of the brainstem, cerebellar white matter and subcortical white matter. Finally, we did not investigate brain structural – function correlates and the discussion of such are thus based on known anatomical – functional and disease – structural correlates.

The main strength of this study was the representative, prospective and well-characterized, general population included, scanned on one scanner with the same protocol, the multiparametric analysis approach, and the high consistency manual WMH delineation. We used high-quality image normalization (Klein et al., 2009) corrected for potential inaccuracies due to image normalization (Battaglini et al., 2012; Sdika and Pelletier, 2009). Spatial statistics was done with a non-parametric permutation test, with better false-positive control than parametric models (Silver et al., 2011). The WMH and no-WMH groups were remarkably similar in size, demographic, somatic and psychiatric characteristics (Table 2 and Supplementary Table 1). Although age and sex differed significantly between the two groups in the volumetric analysis (only age differed in the DTI analysis), the difference was only 1.6 years, and since we corrected for age in the analyses, it is unlikely that the age difference had a notable impact on the results.

5. Conclusion

We show how regional brain volumes and white matter microstructure were associated with presence of WMH and with WMH load in a large sample of community-dwelling people. Major novel findings were that even age normative WMH (i.e. Fazekas grade 1) was indicative of widespread macro- and microstructural changes in gray and white matter, showing that the mere presence of WMH, not just WMH load is an important clinical indicator of brain health. With increasing WMH load, structural changes spread centrifugally. Further, we found three major patterns of FA and MD changes related to increasing WMH load, demonstrating a differential effect on tissue microstructure, where distinct patterns were found in the proximity of the lesions, in deep white

matter and in white matter near the cortex. This study also raises several questions about the onset of WMH related pathology, in particular, whether some of the aberrant brain structural and microstructural findings are present before the emergence of WMH, either emerging before the overt lesions or even representing pleiotropic effects. We also found, similar to other studies, that WMH risk factors had low explanatory power for WMH, making it unclear which factors lead to WMH. Future longitudinal studies of WMH before the emergence of lesions will be needed to address these questions.

Appendix A. Supplementary data

Supplementary data to this article can be found online at https://doi.org/10.1016/j.neuroimage.2019.116158.

References

Al-Mashhadi, S., Simpson, J.E., Heath, P.R., Dickman, M., Forster, G., Matthews, F.E., Brayne, C., Ince, P.G., Wharton, S.B., 2015. Oxidative glial cell damage associated with white matter lesions in the aging human brain. Brain Pathol. 25, 565–574. https://doi.org/10.1111/bpa.12216.

Arshad, M., Stanley, J.A., Raz, N., 2016. Adult age differences in subcortical myelin content are consistent with protracted myelination and unrelated to diffusion tensor imaging indices. Neuroimage 143, 26–39. https://doi.org/10.1016/j.neuroimage.2016.08.047.

Arvanitakis, Z., Fleischman, D.a., Arfanakis, K., Leurgans, S.E., Barnes, L.L., Bennett, D.a., 2016. Association of white matter hyperintensities and gray matter volume with cognition in older individuals without cognitive impairment. Brain Struct. Funct. 221, 2135–2146. https://doi.org/10.1007/s00429-015-1034-7.

Ashburner, J., Friston, K.J., 2004. Chapter 36 - morphometry. In: Human Brain Function. Elsevier, pp. 707–722. https://doi.org/10.1016/B978-012264841-0/50038-X.

Au, R., Massaro, J.M., Wolf, P.A., Young, M.E., Beiser, A., Seshadri, S., D'Agostino, R.B., DeCarli, C., 2006. Association of white matter hyperintensity volume with decreased cognitive functioning. Arch. Neurol. 63, 246. https://doi.org/10.1001/archneur.63.2.246.

Avants, B.B., Epstein, C.L., Grossman, M., Gee, J.C., 2008. Symmetric diffeomorphic image registration with cross-correlation: evaluating automated labeling of elderly and neurodegenerative brain. Med. Image Anal. 12, 26–41. https://doi.org/10.1016/j.media.2007.06.004.

Bansal, S., Buring, J.E., Rifai, N., Mora, S., Sacks, F.M., Ridker, P.M., 2007. Fasting compared with nonfasting triglycerides and risk of cardiovascular events in women. J. Am. Med. Assoc. 298, 309–316. https://doi.org/10.1001/jama.298.3.309.

Bastin, M.E., Clayden, J.D., Pattie, A., Gerrish, I.F., Wardlaw, J.M., Deary, I.J., 2009. Diffusion tensor and magnetization transfer MRI measurements of periventricular white matter hyperintensities in old age. Neurobiol. Aging 30, 125–136. https://doi.org/10.1016/j.neurobiolaging.2007.05.013.

Battaglini, M., Jenkinson, M., De Stefano, N., 2012. Evaluating and reducing the impact of white matter lesions on brain volume measurements. Hum. Brain Mapp. 33, 2062–2071. https://doi.org/10.1002/hbm.21344.

Behrens, T.E.J., Johansen-Berg, H., Woolrich, M.W., Smith, S.M., Wheeler-Kingshott, C.A.M., Boulby, P.A., Barker, G.J., Sillery, E.L., Sheehan, K., Ciccarelli, O., Thompson, A.J., Brady, J.M., Matthews, P.M., 2003. Non-invasive mapping of connections between human thalamus and cortex using diffusion imaging. Nat. Neurosci. 6, 750–757. https://doi.org/10.1038/nn1075.

Bjerkeset, O., Romild, U., Smith, G.D., Hveem, K., 2011. The associations of high levels of C-reactive protein with depression and myocardial infarction in 9258 women and men from the HUNT population study. Psychol. Med. 41, 345–352. https://doi.org/10.1017/S0033291710000887.

Bolandzadeh, N., Liu-Ambrose, T., Aizenstein, H., Harris, T., Launer, L., Yaffe, K., Kritchevsky, S.B., Newman, A., Rosano, C., 2014. Pathways linking regional hyperintensities in the brain and slower gait. Neuroimage 99, 7–13. https://doi.org/10.1016/j.neuroimage.2014.05.017.

Brickman, A.M., Siedlecki, K.L., Muraskin, J., Manly, J.J., Luchsinger, J. a, Yeung, L.-K., Brown, T.R., DeCarli, C., Stern, Y., 2011. White matter hyperintensities and cognition: testing the reserve hypothesis. Neurobiol. Aging 32, 1588–1598. https://doi.org/10.1016/j.neurobiolaging.2009.10.013.

Brickman, A.M., Provenzano, F.A., Muraskin, J., Manly, J.J., Blum, S., Apa, Z., Stern, Y., Brown, T.R., Luchsinger, J.A., Mayeux, R., 2012. Regional white matter hyperintensity volume, not hippocampal atrophy, predicts incident Alzheimer disease in the community. Arch. Neurol. 69, 1621–1627. https://doi.org/10.1001/archneurol.2012.1527.

Brickman, A.M., Zahodne, L.B., Guzman, V.A., Narkhede, A., Meier, I.B., Griffith, E.Y., Provenzano, F.A., Schupf, N., Manly, J.J., Stern, Y., Luchsinger, J.A., Mayeux, R., 2015. Reconsidering harbingers of dementia: progression of parietal lobe white matter hyperintensities predicts Alzheimer's disease incidence. Neurobiol. Aging 36, 27–32. https://doi.org/10.1016/j.neurobiolaging.2014.07.019.

Canty, A., Ripley, B.D., 2017. Boot: Bootstrap R (S-Plus) Functions.

Chau, J.Y., Grunseit, A., Midthjell, K., Holmen, J., Holmen, T.L., Bauman, A.E., van der Ploeg, H.P., 2014. Cross-sectional associations of total sitting and leisure screen time with cardiometabolic risk in adults. Results from the HUNT Study, Norway. J. Sci. Med. Sport 17, 78–84. https://doi.org/10.1016/j.jsams.2013.03.004.

Cherbuin, N., Wen, W., Sachdev, P.S., Anstey, K.J., 2015. Fasting blood glucose levels are associated with white matter hyperintensities' burden in older individuals with and without type 2 diabetes. J. Neurol. Sci. 357, e44. https://doi.org/10.1016/j.jns.2015.08.189.

Concha, L., Gross, D.W., Wheatley, B.M., Beaulieu, C., 2006. Diffusion tensor imaging of time-dependent axonal and myelin degradation after corpus callosotomy in epilepsy patients. Neuroimage 32, 1090–1099. https://doi.org/10.1016/j.neuroimage.2006.04.187.

Cox, S.R., Ritchie, S.J., Tucker-Drob, E.M., Liewald, D.C., Hagenaars, S.P., Davies, G., Wardlaw, J.M., Gale, C.R., Bastin, M.E., Deary, I.J., 2016. Ageing and brain white matter structure in 3,513 UK Biobank participants. Nat. Commun. 7, 13629. https://doi.org/10.1038/ncomms13629.

Dadar, M., Maranzano, J., Misquitta, K., Anor, C.J., Fonov, V.S., Tartaglia, M.C., Carmichael, O.T., Decarli, C., Collins, D.L., 2017. Performance comparison of 10 different classification techniques in segmenting white matter hyperintensities in aging. Neuroimage 157, 233–249. https://doi.org/10.1016/j.neuroimage.2017.06.009.

de Groot, M., Verhaaren, B.F.J., de Boer, R., Klein, S., Hofman, A., van der Lugt, A., Ikram, M.A., Niessen, W.J., Vernooij, M.W., 2013. Changes in normal-appearing white matter precede development of white matter lesions. Stroke 44, 1037–1042. https://doi.org/10.1161/STROKEAHA.112.680223.

de Jong, L.W., van der Hiele, K., Veer, I.M., Houwing, J.J., Westendorp, R.G.J., Bollen, E.L.E.M., de Bruin, P.W., Middelkoop, H.A.M., van Buchem, M.A., van der Grond, J., 2008. Strongly reduced volumes of putamen and thalamus in Alzheimer's disease: an MRI study. Brain 131, 3277–3285. https://doi.org/10.1093/brain/awn278.

de Laat, K.F., Tuladhar, A.M., van Norden, A.G.W., Norris, D.G., Zwiers, M.P., de Leeuw, F.-E., 2011. Loss of white matter integrity is associated with gait disorders in cerebral small vessel disease. Brain 134, 73–83. https://doi.org/10.1093/brain/awq343.

de Leeuw, F.E., de Groot, J.C., Achten, E., Oudkerk, M., Ramos, L.M., Heijboer, R., Hofman, A., Jolles, J., van Gijn, J., Breteler, M.M., 2001. Prevalence of cerebral white matter lesions in elderly people: a population based magnetic resonance imaging study. The Rotterdam scan study. J. Neurol. Neurosurg. Psychiatry 70, 9–14.

Debette, S., Markus, H.S., 2010. The clinical importance of white matter hyperintensities on brain magnetic resonance imaging: systematic review and meta-analysis. BMJ 341, c3666. https://doi.org/10.1136/bmj.c3666.

Desikan, R.S., Fischl, B., Cabral, H.J., Kemper, T.L., Guttmann, C.R.G., Blacker, D., Hyman, B.T., Albert, M.S., Killiany, R.J., 2008. MRI measures of temporoparietal regions show differential rates of atrophy during prodromal AD. Neurology 71, 819–825. https://doi.org/10.1212/01.wnl.0000320055.57329.34.

Dickie, D.A., Karama, S., Ritchie, S.J., Cox, S.R., Sakka, E., Royle, N.A., Aribisala, B.S., Hernández, M.V., Maniega, S.M., Pattie, A., Corley, J., Starr, J.M., Bastin, M.E., Evans, A.C., Deary, I.J., Wardlaw, J.M., 2016a. Progression of white matter disease and cortical thinning are not related in older community-dwelling subjects. Stroke 47, 410–416. https://doi.org/10.1161/STROKEAHA.115.011229.

Dickie, D.A., Ritchie, S.J., Cox, S.R., Sakka, E., Royle, N.A., Aribisala, B.S., Valdés Hernández, M. del C., Maniega, S.M., Pattie, A., Corley, J., Starr, J.M., Bastin, M.E., Deary, I.J., Wardlaw, J.M., 2016b. Vascular risk factors and progression of white matter hyperintensities in the Lothian Birth Cohort 1936. Neurobiol. Aging 42, 116–123. https://doi.org/10.1016/j.neurobiolaging.2016.03.011.

Dufouil, C., Satizabal, C.L., Tzourio, C., Mazoyer, B., Zhu, Y.C., 2012. Circulating IL-6 and CRP are associated with MRI findings in the elderly: the 3C-Dijon study. Neurology 78, 720–727. https://doi.org/10.1212/wnl.0b013e318248e50f.

Eikenes, L., Løhaugen, G.C., Brubakk, A.-M., Skranes, J., Håberg, A.K., 2011. Young adults born preterm with very low birth weight demonstrate widespread white matter alterations on brain DTI. Neuroimage 54, 1774–1785. https://doi.org/10.1016/j.neuroimage.2010.10.037.

Ferreira, D., Hansson, O., Barroso, J., Molina, Y., Machado, A., Hernández-Cabrera, J.A., Muehlboeck, J.-S., Stomrud, E., Nägga, K., Lindberg, O., Ames, D., Kalpouzos, G., Fratiglioni, L., Bäckman, L., Graff, C., Mecocci, P., Vellas, B., Tsolaki, M., Kłoszewska, I., Soininen, H., Lovestone, S., Ahlström, H., Lind, L., Larsson, E.-M., Wahlund, L.-O., Simmons, A., Westman, E., for the AddNeuroMed consortium, for the A.D.N.I. (ADNI), Australian Imaging Biomarkers and Lifestyle Study of Ageing (AIBL) research group, 2017. The interactive effect of demographic and clinical factors on hippocampal volume: a multicohort study on 1958 cognitively normal individuals. Hippocampus 27, 653–667. https://doi.org/10.1002/hipo.22721.

Fazekas, F., Chawluk, J., Alavi, A., Hurtig, H., Zimmerman, R., 1987. MR signal abnormalities at 1.5 T in Alzheimer's dementia and normal aging. Am. J. Roentgenol. 149, 351.

Fazekas, F., Kleinert, R., Offenbacher, H., Schmidt, R., Kleinert, G., Payer, F., Radner, H., Lechner, H., 1993. Pathologic correlates of incidental MRI white matter signal hyperintensities. Neurology 43, 1683–1689.

Fazekas, F., Ropele, S., Enzinger, C., Gorani, F., Seewann, A., Petrovic, K., Schmidt, R., 2005. MTI of white matter hyperintensities. Brain 128, 2926–2932. https://doi.org/10.1093/brain/awh567.

Fernando, M.S., Ince, P.G., 2004. Vascular pathologies and cognition in a population-based cohort of elderly people. J. Neurol. Sci. 226, 13–17. https://doi.org/10.1016/j.jns.2004.09.004.

Fernando, M.S., Simpson, J.E., Matthews, F., Brayne, C., Lewis, C.E., Barber, R., Kalaria, R.N., Forster, G., Esteves, F., Wharton, S.B., Shaw, P.J., O'Brien, J.T., Ince, P.G., 2006. White matter lesions in an unselected cohort of the elderly. Stroke 37, 1391–1398. https://doi.org/10.1161/01.STR.0000221308.94473.14.

Gouw, A.A., Van der Flier, W.M., van Straaten, E.C.W., Barkhof, F., Ferro, J.M., Baezner, H., Pantoni, L., Inzitari, D., Erkinjuntti, T., Wahlund, L.O., Waldemar, G., Schmidt, R., Fazekas, F., Scheltens, P., 2006. Simple versus complex assessment of white matter hyperintensities in relation to physical performance and cognition: the LADIS study. J. Neurol. 253, 1189–1196. https://doi.org/10.1007/s00415-006-0193-5.

Gouw, A.A., Seewann, A., van der Flier, W.M., Barkhof, F., Rozemuller, A.M., Scheltens, P., Geurts, J.J.G., 2011. Heterogeneity of small vessel disease: a systematic review of MRI and histopathology correlations. J. Neurol. Neurosurg. Psychiatry 82, 126–135. https://doi.org/10.1136/jnnp.2009.204685.

Håberg, A.K., Olsen, A., Moen, K.G., Schirmer-Mikalsen, K., Visser, E., Finnanger, T.G., Evensen, K.A.I., Skandsen T., Vik, A., Eikenes, L., 2015. White matter microstructure in chronic moderate-to-severe traumatic brain injury: impact of acute-phase injury-related variables and associations with outcome measures. J. Neurosci. Res. 93, 1109–1126. https://doi.org/10.1002/jnr.23534.

Håberg, A.K., Hammer, T.A., Kvistad, K.A., Rydland, J., Müller, T.B., Eikenes, L., Gårseth, M., Stovner, L.J., 2016. Incidental intracranial findings and their clinical impact; the HUNT MRI study in a general population of 1006 participants between 50-66 years. PLoS One 11, e0151080. https://doi.org/10.1371/journal.pone.0151080.

Habes, M., Erus, G., Toledo, J.B., Zhang, T., Bryan, N., Launer, L.J., Rosseel, Y., Janowitz, D., Doshi, J., Van der Auwera, S., von Sarnowski, B., Hegenscheid, K., Hosten, N., Homuth, G., Völzke, H., Schminke, U., Hoffmann, W., Grabe, H.J., Davatzikos, C., 2016. White matter hyperintensities and imaging patterns of brain ageing in the general population. Brain 139, 1164–1179. https://doi.org/10.1093/brain/aww008.

Hansen, T.I., Brezova, V., Eikenes, L., Haberg, A., Vangberg, T.R., 2015. How does the accuracy of intracranial volume measurements affect normalized brain volumes? Sample size estimates based on 966 subjects from the HUNT MRI cohort. Am. J. Neuroradiol. 36, 1450–1456. https://doi.org/10.3174/ajnr.A4299.

Hibar, D.P., Adams, H.H.H., Jahanshad, N., Chauhan, G., Stein, J.L., Hofer, E., et al., 2017. Novel genetic loci associated with hippocampal volume. Nat. Commun. 8, 13624. https://doi.org/10.1038/ncomms13624.

Hill, S.Y., Lichenstein, S., Wang, S., Carter, H., McDermott, M., 2013. Caudate volume in offspring at ultra high risk for alcohol dependence: COMT Val158Met, DRD2, externalizing disorders, and working memory. Adv. Mol. Imag. 3, 43–54. https://doi.org/10.4236/ami.2013.34007.

Holmen, J., Midthjell, K., Kruger, O., Langhammer, A., Holmen, T., Bratberg, G., 2003. The Nord-Trondelag Health Study 1995-97 (HUNT2): objectives, contents, methods and participation. Nor. J. Epidemiol. 13, 19–32.

Honningsvåg, L.-M., Linde, M., Håberg, A., Stovner, L.J., Hagen, K., 2012. Does health differ between participants and non-participants in the MRI-HUNT study, a population based neuroimaging study? The Nord-Trøndelag health studies 1984-2009. BMC Med. Imaging 12, 23. https://doi.org/10.1186/1471-2342-12-23.

Hoogendam, Y.Y., van der Geest, J.N., van der Lijn, F., van der Lugt, A., Niessen, W.J., Krestin, G.P., Hofman, A., Vernooij, M.W., Breteler, M.M.B., Ikram, M.A., 2012. Determinants of cerebellar and cerebral volume in the general elderly population. Neurobiol. Aging 33, 2774–2781. https://doi.org/10.1016/j.neurobiolaging.2012.02.012.

Hopkins, R.O., Beck, C.J., Burnett, D.L., Weaver, L.K., Victoroff, J., Bigler, E.D., 2006. Prevalence of white matter hyperintensities in a young healthy population. J. Neuroimaging 16, 243–251. https://doi.org/10.1111/j.1552-6569.2006.00047.x.

Hua, K., Zhang, J., Wakana, S., Jiang, H., Li, X., Reich, D.S., Calabresi, P.A., Pekar, J.J., van Zijl, P.C.M., Mori, S., 2008. Tract probability maps in stereotaxic spaces: analyses of white matter anatomy and tract-specific quantification. Neuroimage 39, 336–347. https://doi.org/10.1016/j.neuroimage.2007.07.053.

Ikram, M.A., Vrooman, H.A., Vernooij, M.W., van der Lijn, F., Hofman, A., van der Lugt, A., Niessen, W.J., Breteler, M.M.B., 2008. Brain tissue volumes in the general elderly population. The Rotterdam Scan Study. Neurobiol. Aging 29, 882–890. https://doi.org/10.1016/j.neurobiolaging.2006.12.012.

Inzitari, D., Simoni, M., Pracucci, G., Poggesi, A., Basile, A.M., Chabriat, H., Erkinjuntti, T., Fazekas, F., Ferro, J.M., Hennerici, M., Langhorne, P., O'Brien, J., Barkhof, F., Visser, M.C., Wahlund, L.-O., Waldemar, G., Wallin, A., Pantoni, L.,

LADIS Study Group, 2007. Risk of rapid global functional decline in elderly patients with severe cerebral age-related white matter changes: the LADIS study. Arch. Intern. Med. 167, 81–88. https://doi.org/10.1001/archinte.167.1.81.

Inzitari, D., Pracucci, G., Poggesi, A., Carlucci, G., Barkhof, F., Chabriat, H., Erkinjuntti, T., Fazekas, F., Ferro, J.M., Hennerici, M., Langhorne, P., O'Brien, J., Scheltens, P., Visser, M.C., Wahlund, L., Waldemar, G., Wallin, A., Pantoni, L., 2009. Changes in white matter as determinant of global functional decline in older independent outpatients: three year follow-up of LADIS (leukoaraiosis and disability) study cohort. BMJ 339, b2477. https://doi.org/10.1136/bmj.b2477.

Jacobs, H.I.L., Van Boxtel, M.P.J., Jolles, J., Verhey, F.R.J., Uylings, H.B.M., 2012. Parietal cortex matters in Alzheimer's disease: an overview of structural, functional and metabolic findings. Neurosci. Biobehav. Rev. 36, 297–309. https://doi.org/10.10 16/j.neubiorev.2011.06.009.

Jeerakathil, T., Wolf, P.A., Beiser, A., Massaro, J., Seshadri, S., D'Agostino, R.B., DeCarli, C., 2004. Stroke risk profile predicts white matter hyperintensity volume: the Framingham study. Stroke 35, 1857–1861. https://doi.org/10.1161/01.STR. 0000135226.53499.85.

Kale, R.A., Gupta, R.K., Saraswat, V.A., Hasan, K.M., Trivedi, R., Mishra, A.M., Ranjan, P., Pandey, C.M., Narayana, P.A., 2006. Demonstration of interstitial cerebral edema with diffusion tensor MR imaging in type C hepatic encephalopathy. Hepatology 43, 698–706. https://doi.org/10.1002/hep.21114.

King, K.S., Peshock, R.M., Rossetti, H.C., McColl, R.W., Ayers, C.R., Hulsey, K.M., Das, S.R., 2014. Effect of normal aging versus hypertension, abnormal body mass index, and diabetes mellitus on white matter hyperintensity volume. Stroke 45, 255–257. https://doi.org/10.1161/STROKEAHA.113.003602.

Klein, A., Andersson, J., Ardekani, B.A., Ashburner, J., Avants, B., Chiang, M., Christensen, G.E., Collins, D.L., Gee, J., Hellier, P., Song, J.H., Jenkinson, M., Lepage, C., Rueckert, D., Thompson, P., Vercauteren, T., Woods, R.P., Mann, J.J., Parsey, R.V., 2009. Evaluation of 14 nonlinear deformation algorithms applied to human brain MRI registration. Neuroimage 46, 786–802. https://doi.org/10.1016/j. neuroimage.2008.12.037.

Kreczmanski, P., Heinsen, H., Mantua, V., Woltersdorf, F., Masson, T., Ulfig, N., Schmidt-Kastner, R., Korr, H., Steinbusch, H.W.M., Hof, P.R., Schmitz, C., 2007. Volume, neuron density and total neuron number in five subcortical regions in schizophrenia. Brain 130, 678–692. https://doi.org/10.1093/brain/awl386.

Krokstad, S., Langhammer, A., Hveem, K., Holmen, T.L., Midthjell, K., Stene, T.R., Bratberg, G., Heggland, J., Holmen, J., 2013. Cohort profile: the HUNT study, Norway. Int. J. Epidemiol. 42, 968–977. https://doi.org/10.1093/ije/dys095.

Lebedeva, A.K., Westman, E., Borza, T., Beyer, M.K., Engedal, K., Aarsland, D., Selbaek, G., Haberg, A.K., 2017. MRI-based classification models in prediction of mild cognitive impairment and dementia in late-life depression. Front. Aging Neurosci. 9, 1–11. https://doi.org/10.3389/fnagi.2017.00013.

Lee, S., Viqar, F., Zimmerman, M.E., Narkhede, A., Tosto, G., Benzinger, T.L.S., Marcus, D.S., Fagan, A.M., Goate, A., Fox, N.C., Cairns, N.J., Holtzman, D.M., Buckles, V., Ghetti, B., McDade, E., Martins, R.N., Saykin, A.J., Masters, C.L., Ringman, J.M., Ryan, N.S., Förster, S., Laske, C., Schofield, P.R., Sperling, R.A., Salloway, S., Correia, S., Jack, C., Weiner, M., Bateman, R.J., Morris, J.C., Mayeux, R., Brickman, A.M., 2016. White matter hyperintensities are a core feature of Alzheimer's disease: evidence from the dominantly inherited Alzheimer network. Ann. Neurol. 79, 929–939. https://doi.org/10.1002/ana.24647.

Leow, A.D., Yanovsky, I., Chiang, M.C., Lee, A.D., Klunder, A.D., Lu, A., Becker, J.T., Davis, S.W., Toga, A.W., Thompson, P.M., 2007. Statistical properties of Jacobian maps and the ralization of unbiased large-deformation nonlinear image registration. IEEE Trans. Med. 26, 822–832. https://doi.org/10.1109/TMI.2007.892646.

Leritz, E.C., Shepel, J., Williams, V.J., Lipsitz, L.A., McGlinchey, R.E., Milberg, W.P., Salat, D.H., 2014. Associations between T1 white matter lesion volume and regional white matter microstructure in aging. Hum. Brain Mapp. 35, 1085–1100. https:// doi.org/10.1002/hbm.22236.

Lindemer, E.R., Salat, D.H., Smith, E.E., Nguyen, K., Fischl, B., Greve, D.N., 2015. White matter signal abnormality quality differentiates mild cognitive impairment that converts to Alzheimer's disease from nonconverters. Neurobiol. Aging 36, 2447–2457. https://doi.org/10.1016/j.neurobiolaging.2015.05.011.

Liu, M.-E., Huang, C.-C., Yang, A.C., Tu, P.-C., Yeh, H.-L., Hong, C.-J., Liou, Y.-J., Chen, J.-F., Chou, K.-H., Lin, C.-P., Tsai, S.-J., 2014. Catechol-O-Methyltransferase Val158Met polymorphism on the relationship between white matter hyperintensity and cognition in healthy people. PLoS One 9, e88749. https://doi.org/10.1371/journ al.pone.0088749.

Love, S., Miners, J.S., 2016. Cerebrovascular disease in ageing and Alzheimer's disease. Acta Neuropathol. 131, 645–658. https://doi.org/10.1007/s00401-015-1522-0.

Maillard, P., Fletcher, E., Harvey, D., Carmichael, O., Reed, B., Mungas, D., DeCarli, C., 2011. White matter hyperintensity penumbra. Stroke 42, 1917–1922. https://doi.org /10.1161/STROKEAHA.110.609768.

Maillard, P., Carmichael, O., Fletcher, E., Reed, B., Mungas, D., DeCarli, C., 2012. Coevolution of white matter hyperintensities and cognition in the elderly. Neurology 79, 442–448. https://doi.org/10.1212/WNL.0b013e3182617136.

Maillard, P., Carmichael, O., Harvey, D., Fletcher, E., Reed, B., Mungas, D., DeCarli, C., 2013. FLAIR and diffusion MRI signals are independent predictors of white matter hyperintensities. AJNR (Am. J. Neuroradiol.) 34, 54–61. https://doi.org/10.3174/a jnr.A3146.

Maillard, P., Fletcher, E., Lockhart, S.N., Roach, A.E., Reed, B., Mungas, D., Decarli, C., Carmichael, O.T., 2014. White matter hyperintensities and their penumbra lie along a continuum of injury in the aging brain. Stroke 45, 1721–1726. https://doi.org/10.11 61/STROKEAHA.113.004084.

Maniega, S.M., Valdés Hernández, M.C., Clayden, J.D., Royle, N.A., Murray, C., Morris, Z., Aribisala, B.S., Gow, A.J., Starr, J.M., Bastin, M.E., Deary, I.J., Wardlaw, J.M., 2015. White matter hyperintensities and normal-appearing white matter integrity in the aging brain. Neurobiol. Aging 36, 909–918. https://doi.org/10.1016/j.neurobiolagi ng.2014.07.048.

McAleese, K.E., Firbank, M., Dey, M., Colloby, S.J., Walker, L., Johnson, M., Beverley, J.R., Taylor, J.P., Thomas, A.J., O'Brien, J.T., Attems, J., 2015. Cortical tau load is associated with white matter hyperintensities. Acta Neuropathol. Commun. 3, 60. https://doi.org/10.1186/s40478-015-0240-0.

McAleese, K.E., Walker, L., Graham, S., Moya, E.L.J., Johnson, M., Erskine, D., Colloby, S.J., Dey, M., Martin-Ruiz, C., Taylor, J.-P., Thomas, A.J., McKeith, I.G., De Carli, C., Attems, J., 2017. Parietal white matter lesions in Alzheimer's disease are associated with cortical neurodegenerative pathology, but not with small vessel disease. Acta Neuropathol. 134, 459–473. https://doi.org/10.1007/s00401-0 17-1738-2.

Murray, M.E., Senjem, M.L., Petersen, R.C., Hollman, J.H., Preboske, G.M., Weigand, S.D., Knopman, D.S., Ferman, T.J., Dickson, D.W., Jack, C.R., 2010. Functional impact of white matter hyperintensities in cognitively normal elderly subjects. Arch. Neurol. 67, 1379–1385. https://doi.org/10.1001/archneurol.2010.280.

Murray, M.E., Vemuri, P., Preboske, G.M., Murphy, M.C., Schweitzer, K.J., Parisi, J.E., Jack, C.R., Dickson, D.W., 2012. A quantitative postmortem MRI design sensitive to white matter hyperintensity differences and their relationship with underlying pathology. J. Neuropathol. Exp. Neurol. 71, 1113–1122. https://doi.org/10.1097/N EN.0b013e318277387e.

Nestor, S.M., Rupsingh, R., Borrie, M., Smith, M., Accomazzi, V., Wells, J.L., Fogarty, J., Bartha, R., Alzheimer's Disease Neuroimaging Initiative, 2008. Ventricular enlargement as a possible measure of Alzheimer's disease progression validated using the Alzheimer's disease neuroimaging initiative database. Brain 131, 2443–2454. https://doi.org/10.1093/brain/awn146.

Nyquist, P.A., Bilgel, M., Gottesman, R., Yanek, L.R., Moy, T.F., Becker, L.C., Cuzzocreo, J.L., Prince, J., Wasserman, B.A., Yousem, D.M., Becker, D.M., Kral, B.G., Vaidya, D., 2015. Age differences in periventricular and deep white matter lesions. Neurobiol. Aging 36, 1653–1658. https://doi.org/10.1016/j.neurobiolaging.2015.0 1.005.

O'Brien, J.T., Thomas, A., 2015. Vascular dementia. Lancet 386, 1698–1706. https://doi.org/10.1016/S0140-6736(15)00463-8.

Parker, T.D., Slattery, C.F., Zhang, J., Nicholas, J.M., Paterson, R.W., Foulkes, A.J.M., Malone, I.B., Thomas, D.L., Modat, M., Cash, D.M., Crutch, S.J., Alexander, D.C., Ourselin, S., Fox, N.C., Zhang, H., Schott, J.M., 2018. Cortical microstructure in young onset Alzheimer's disease using neurite orientation dispersion and density imaging. Hum. Brain Mapp. 39, 3005–3017. https://doi.org/10.1002/hbm.24056.

Persson, K., Bohbot, V.D., Bogdanovic, N., Selbæk, G., Brækhus, A., Engedal, K., 2018. Finding of increased caudate nucleus in patients with Alzheimer's disease. Acta Neurol. Scand. 137, 224–232. https://doi.org/10.1111/ane.12800.

Pinter, D., Ritchie, S.J., Doubal, F., Gattringer, T., Morris, Z., Bastin, M.E., Hernández, M.D.C.V., Royle, N.A., Corley, J., Muñoz Maniega, S., Pattie, A., Dickie, D.A., Staals, J., Gow, A.J., Starr, J.M., Deary, I.J., Enzinger, C., Fazekas, F., Wardlaw, J., 2017. Impact of small vessel disease in the brain on gait and balance. Sci. Rep. 7, 1–8. https://doi.org/10.1038/srep41637.

Promjunyakul, N., Lahna, D., Kaye, J.a.A., Dodge, H.H.H., Erten-Lyons, D., Rooney, W.D.D., Silbert, L.C.C., 2015. Characterizing the white matter hyperintensity penumbra with cerebral blood flow measures. Neuroimage Clin. 8, 224–229. htt ps://doi.org/10.1016/j.nicl.2015.04.012.

R Core Team, 2017. R: A Language and Environment for Statistical Computing.

Raji, C. a, Lopez, O.L., Kuller, L.H., Carmichael, O.T., Longstreth, W.T., Gach, H.M., Boardman, J., Bernick, C.B., Thompson, P.M., Becker, J.T., 2012. White matter lesions and brain gray matter volume in cognitively normal elders. Neurobiol. Aging 33, 834 e7–16. https://doi.org/10.1016/j.neurobiolaging.2011.08.010.

Rostrup, E., Gouw, A.A., Vrenken, H., van Straaten, E.C.W., Ropele, S., Pantoni, L., Inzitari, D., Barkhof, F., Waldemar, G., 2012. The spatial distribution of age-related white matter changes as a function of vascular risk factors—results from the LADIS study. Neuroimage 60, 1597–1607. https://doi.org/10.1016/j.neuroimage.2012.01. 106.

Sachdev, P.S., 2005. White matter hyperintensities are related to physical disability and poor motor function. J. Neurol. Neurosurg. Psychiatry 76, 362–367. https://doi .org/10.1136/jnnp.2004.042945.

Schmidt, R., Ropele, S., Enzinger, C., Petrovic, K., Smith, S., Schmidt, H., Matthews, P.M., Fazekas, F., 2005. White matter lesion progression, brain atrophy, and cognitive decline: the Austrian stroke prevention study. Ann. Neurol. 58, 610–616. https:// doi.org/10.1002/ana.20630.

Schwarz, C.G., Senjem, M.L., Gunter, J.L., Tosakulwong, N., Weigand, S.D., Kemp, B.J., Spychalla, A.J., Vemuri, P., Petersen, R.C., Lowe, V.J., Jack, C.R., 2017. Optimizing PiB-PET SUVR change-over-time measurement by a large-scale analysis of longitudinal reliability, plausibility, separability, and correlation with MMSE. Neuroimage 144, 113–127. https://doi.org/10.1016/j.neuroimage.2016.08.056.

Scott, J.A., Braskie, M.N., Tosun, D., Thompson, P.M., Weiner, M., DeCarli, C., Carmichael, O.T., 2015. Cerebral amyloid and hypertension are independently associated with white matter lesions in elderly. Front. Aging Neurosci. 7, 1–9. https://doi.org/10.3389/fnagi.2015.00221.

Scott, J.A., Braskie, M.N., Tosun, D., Maillard, P., Thompson, P.M., Weiner, M., DeCarli, C., Carmichael, O.T., 2016. Cerebral amyloid is associated with greater white-matter hyperintensity accrual in cognitively normal older adults. Neurobiol. Aging 48, 48–52. https://doi.org/10.1016/j.neurobiolaging.2016.08.014.

Sdika, M., Pelletier, D., 2009. Nonrigid registration of multiple sclerosis brain images using lesion inpainting for morphometry or lesion mapping. Hum. Brain Mapp. 30, 1060–1067. https://doi.org/10.1002/hbm.20566.

Silbert, L.C., Nelson, C., Howieson, D.B., Moore, M.M., Kaye, J. a, 2008. Impact of white matter hyperintensity volume progression on rate of cognitive and motor decline. Neurology 71, 108–113. https://doi.org/10.1212/01.wnl.0000316799.86917.37.

Silver, M., Montana, G., Nichols, T.E., 2011. False positives in neuroimaging genetics using voxel-based morphometry data. Neuroimage 54, 992–1000. https://doi.org/10.1016/j.neuroimage.2010.08.049.

Simpson, J.E., Ince, P.G., Higham, C.E., Gelsthorpe, C.H., Fernando, M.S., Matthews, F., Forster, G., O'Brien, J.T., Barber, R., Kalaria, R.N., Brayne, C., Shaw, P.J., Stoeber, K., Williams, G.H., Lewis, C.E., Wharton, S.B., 2007. Microglial activation in white matter lesions and nonlesional white matter of ageing brains. Neuropathol. Appl. Neurobiol. 33, 670–683. https://doi.org/10.1111/j.1365-2990.2007.00890.x.

Smith, S.M., Nichols, T.E., 2009. Threshold-free cluster enhancement: addressing problems of smoothing, threshold dependence and localisation in cluster inference. Neuroimage 44, 83–98. https://doi.org/10.1016/j.neuroimage.2008.03.061.

Smith, E.E., Salat, D.H., Jeng, J., McCreary, C.R., Fischl, B., Schmahmann, J.D., Dickerson, B.C., Viswanathan, A., Albert, M.S., Blacker, D., Greenberg, S.M., 2011. Correlations between MRI white matter lesion location and executive function and episodic memory. Neurology 76, 1492–1499. https://doi.org/10.1212/WNL.0b013e318217e7c8.

Smith, E.E., O'Donnell, M., Dagenais, G., Lear, S.A., Wielgosz, A., Sharma, M., Poirier, P., Stotts, G., Black, S.E., Strother, S., Noseworthy, M.D., Benavente, O., Modi, J., Goyal, M., Batool, S., Sanchez, K., Hill, V., McCreary, C.R., Frayne, R., Islam, S., DeJesus, J., Rangarajan, S., Teo, K., Yusuf, S., 2015. Early cerebral small vessel disease and brain volume, cognition, and gait. Ann. Neurol. 77, 251–261. https://doi.org/10.1002/ana.24320.

Stricker, N.H., Schweinsburg, B.C., Delano-Wood, L., Wierenga, C.E., Bangen, K.J., Haaland, K.Y., Frank, L.R., Salmon, D.P., Bondi, M.W., 2009. Decreased white matter integrity in late-myelinating fiber pathways in Alzheimer's disease supports retrogenesis. Neuroimage 45, 10–16. https://doi.org/10.1016/j.neuroimage.2008.11.027.

Taylor, W.D., Jae, N.B., MacFall, J.R., Payne, M.E., Provenzale, J.M., Steffens, D.C., Krishnan, K.R.R., 2007. Widespread effects of hyperintense lesions on cerebral white matter structure. Am. J. Roentgenol. 188, 1695–1704. https://doi.org/10.2214/AJR.06.1163.

Tuladhar, A.M., Reid, A.T., Shumskaya, E., De Laat, K.F., Van Norden, A.G.W., Van Dijk, E.J., Norris, D.G., De Leeuw, F.E., 2014. Relationship between white matter hyperintensities, cortical thickness, and cognition. Stroke. https://doi.org/10.1161/STROKEAHA.114.007146.

Tustison, N.J., Avants, B.B., Cook, P.A., Zheng, Yuanjie, Egan, A., Yushkevich, P.A., Gee, J.C., 2010. N4ITK: improved N3 bias correction. IEEE Trans. Med. Imaging 29, 1310–1320. https://doi.org/10.1109/TMI.2010.2046908.

Tustison, N.J., Avants, B.B., Cook, P. a, Kim, J., Whyte, J., Gee, J.C., Stone, J.R., 2014. Logical circularity in voxel-based analysis: normalization strategy may induce statistical bias. Hum. Brain Mapp. 35, 745–759. https://doi.org/10.1002/hbm.22211.

van Agtmaal, M.J.M., Houben, A.J.H.M., Pouwer, F., Stehouwer, C.D.A., Schram, M.T., 2017. Association of microvascular dysfunction with late-life depression. JAMA Psychiatr. 74, 729. https://doi.org/10.1001/jamapsychiatry.2017.0984.

van den Heuvel, D.M.J., Admiraal-Behloul, F., ten Dam, V.H., Olofsen, H., Bollen, E.L.E.M., Murray, H.M., Blauw, G.J., Westendorp, R.G.J., de Craen, A.J.M., van Buchem, M.A., 2004. Different progression rates for deep white matter hyperintensities in elderly men and women. Neurology 63, 1699–1701. https://doi.org/10.1212/01.WNL.0000143058.40388.44.

van der Veen, P.H., Muller, M., Vincken, K.L., Witkamp, T.D., Mali, W.P.T.M., van der Graaf, Y., Geerlings, M.I., 2014. Longitudinal changes in brain volumes and cerebrovascular lesions on MRI in patients with manifest arterial disease: the SMART-MR study. J. Neurol. Sci. 337, 112–118. https://doi.org/10.1016/j.jns.2013.11.029.

van Dijk, E.J., Breteler, M.M.B., Schmidt, R., Berger, K., Nilsson, L.-G., Oudkerk, M., Pajak, A., Sans, S., de Ridder, M., Dufouil, C., Fuhrer, R., Giampaoli, S., Launer, L.J., Hofman, A., 2004. The association between blood pressure, hypertension, and cerebral white matter lesions: cardiovascular determinants of dementia study. Hypertension 44, 625–630. https://doi.org/10.1161/01.HYP.0000145857.98904.20.

van Dijk, E.J., Prins, N.D., Vrooman, H.A., Hofman, A., Koudstaal, P.J., Breteler, M.M.B., 2008. Progression of cerebral small vessel disease in relation to risk factors and cognitive consequences: Rotterdam scan study. Stroke 39, 2712–2719. https://doi.org/10.1161/STROKEAHA.107.513176.

van Leijsen, E.M.C., Bergkamp, M.I., Uden, I.W.M. van, Ghafoorian, M., Holst, H.M. van der, Norris, D.G., Platel, B., Tuladhar, A.M., Leeuw, F.-E. de, 2018. Progression of white matter hyperintensities preceded by heterogeneous decline of microstructural integrity. Stroke 118, 20980. STROKEAHA. https://doi.org/10.1161/STROKEAHA.118.020980.

Verhaaren, B.F.J., de Boer, R., Vernooij, M.W., Rivadeneira, F., Uitterlinden, A.G., Hofman, A., Krestin, G.P., van der Lugt, A., Niessen, W.J., Breteler, M.M.B., Ikram, M.A., 2011. Replication study of Chr17q25 with cerebral white matter lesion volume. Stroke 42, 3297–3299. https://doi.org/10.1161/STROKEAHA.111.623090.

Vernooij, M.W., Ikram, M.A., Tanghe, H.L., Vincent, A.J.P.E., Hofman, A., Krestin, G.P., Niessen, W.J., Breteler, M.M.B., van der Lugt, A., 2007. Incidental findings on brain MRI in the general population. N. Engl. J. Med. 357, 1821–1828. https://doi.org/10.1056/NEJMoa070972.

Vernooij, M.W., de Groot, M., van der Lugt, A., Ikram, M.A., Krestin, G.P., Hofman, A., Niessen, W.J., Breteler, M.M.B., 2008. White matter atrophy and lesion formation explain the loss of structural integrity of white matter in aging. Neuroimage 43, 470–477. https://doi.org/10.1016/j.neuroimage.2008.07.052.

Vernooij, M.W., Ikram, M.A., Vrooman, H.A., Wielopolski, P.A., Krestin, G.P., Hofman, A., Niessen, W.J., van der Lugt, A., Breteler, M.M.B., 2009. White Matter microstructural integrity and cognitive function in a general elderly population. Arch. Gen. Psychiatr. 66, 545–553. https://doi.org/10.1001/archgenpsychiatry.2009.5.

Wang, R., Fratiglioni, L., Laveskog, A., Kalpouzos, G., Ehrenkrona, C.H., Zhang, Y., Bronge, L., Wahlund, L.O., Bäckman, L., Qiu, C., 2014a. Do cardiovascular risk factors explain the link between white matter hyperintensities and brain volumes in old age? A population-based study. Eur. J. Neurol. 21, 1076–1082. https://doi.org/10.1111/ene.12319.

Wang, L., Leonards, C.O., Sterzer, P., Ebinger, M., 2014b. White matter lesions and depression: a systematic review and meta-analysis. J. Psychiatr. Res. 56, 56–64. https://doi.org/10.1016/j.jpsychires.2014.05.005.

Wardlaw, J.M., Allerhand, M., Doubal, F.N., Morris, Z., Gow, A.J., Bastin, M.E., Starr, J.M., Dennis, M.S., 2014. Vascular risk factors , large-artery atheroma , and brain white matter hyperintensities. Neurology 82, 1331–1338. https://doi.org/10.1212/WNL.0000000000000312.

Wardlaw, J.M., Valdés Hernández, M.C., Muñoz-Maniega, S., 2015. What are white matter hyperintensities made of? Relevance to vascular cognitive impairment. J. Am. Heart Assoc. 4, e001140. https://doi.org/10.1161/JAHA.114.001140.

Wardlaw, J.M., Makin, S.J., Valdés Hernández, M.C., Armitage, P.A., Heye, A.K., Chappell, F.M., Muñoz-Maniega, S., Sakka, E., Shuler, K., Dennis, M.S., Thrippleton, M.J., 2017. Blood-brain barrier failure as a core mechanism in cerebral small vessel disease and dementia: evidence from a cohort study. Alzheimer's Dementia 13, 634–643. https://doi.org/10.1016/j.jalz.2016.09.006.

Wen, W., Sachdev, P.S., Chen, X., Anstey, K., 2006. Gray matter reduction is correlated with white matter hyperintensity volume: a voxel-based morphometric study in a large epidemiological sample. Neuroimage 29, 1031–1039. https://doi.org/10.1016/j.neuroimage.2005.08.057.

Wickham, H., 2011. The split-apply-combine strategy for data. J. Stat. Softw. 40.

Willey, J.Z., Scarmeas, N., Provenzano, F.A., Luchsinger, J.A., Mayeux, R., Brickman, A.M., 2013. White matter hyperintensity volume and impaired mobility among older adults. J. Neurol. 260, 884–890. https://doi.org/10.1007/s00415-012-6731-z.

Winkler, A.M., Ridgway, G.R., Webster, M.a., Smith, S.M., Nichols, T.E., 2014. Permutation inference for the general linear model. Neuroimage 92, 381–397. https://doi.org/10.1016/j.neuroimage.2014.01.060.

Winkler, A.M., Ridgway, G.R., Douaud, G.G., Nichols, T.E., Smith, S.M., 2016. Faster permutation inference in brain imaging. Neuroimage 141, 502–516. https://doi.org/10.1016/j.neuroimage.2016.05.068.

Yee, T.W., 2010. The VGAM package for categorical data analysis. J. Stat. Softw. 32. https://doi.org/10.18637/jss.v032.i10.

Zhang, Y., Du, A.T., Hayasaka, S., Jahng, G. ho, Hlavin, J., Zhan, W., Weiner, M.W., Schuff, N., 2010. Patterns of age-related water diffusion changes in human brain by concordance and discordance analysis. Neurobiol. Aging 31, 1991–2001. https://doi.org/10.1016/j.neurobiolaging.2008.10.009.